# Mesozoic and Cenozoic tectonic evolution of the Shiquanhe area of western Tibet

Paul Kapp,[1] Michael A. Murphy,[2] An Yin, and T. Mark Harrison[3]

Department of Earth and Space Sciences and Institute of Geophysics and Planetary Physics, University of California, Los Angeles, California, USA

Lin Ding and Jinghu Guo

Institute of Geology and Geophysics, Lithosphere Tectonic Evolution Laboratory, Chinese Academy of Sciences, Beijing, People's Republic of China

Received 1 October 2001; revised 26 July 2002; accepted 31 January 2003; published 9 July 2003.

[1] In the Shiquanhe area of far-western Tibet, mid-Cretaceous strata lie unconformable on ophiolitic melange and Jurassic flysch associated with the Bangong-Nujiang suture zone. On the basis of our mapping and geochronologic studies, we suggest that these Cretaceous strata were shortened by >57% over a north south distance of 50 km during Late Cretaceous-early Tertiary time. The Late Cretaceous Narangjiapo thrust placed Permian strata >20 km over ophiolitic melange and Cretaceous strata. North of the Narangjiapo thrust, >40 km of shortening was accommodated by the Late Cretaceous-early Tertiary south directed Jaggang thrust system that involves Jurassic flysch and Cretaceous strata, and roots into a decollement within ophiolitic melange. The most recent shortening was accommodated to the south of the Narangjiapo thrust, along the north dipping Shiquanhe thrust. The Shiquanhe thrust cuts flat-lying 22.6 ± 0.3 Ma volcanic rocks and underlying folded, Tertiary nonmarine strata in its footwall and was likely active during slip along the Oligocene Gangdese thrust system of southern Tibet. Ophiolitic melange and structurally overlying Jurassic flysch near Shiquanhe are interpreted to represent remnants of a subduction-accretion complex and forearc basin, respectively, that were obducted southward onto the margin of the Lhasa terrane during Late Jurassic-Early Cretaceous closure of the Bangong-Nujiang Ocean. Subsequent imbrication of the obducted sheet could have produced the two east-west trending belts of ophiolitic melanges, separated by ~100 km, in western Tibet. Late Cretaceous-early Tertiary thin-skinned shortening may have been accommodated in the deeper crust by northward underthrusting and duplexing of Lhasa terrane rocks beneath the obducted ophiolitic melange and the Qiangtang terrane to the north. *INDEX TERMS:* 8015 Structural Geology: Local crustal structure; 8102 Tectonophysics: Continental contractional orogenic belts; 9320 Information Related to Geographic Region: Asia; 1035 Geochemistry: Geochronology; 9604 Information Related to Geologic Time: Cenozoic; *KEYWORDS:* Tibet, Bangong suture, melange, obduction, underthrusting, plateau formation. **Citation:** Kapp, P., M. A. Murphy, A. Yin, T. M. Harrison, L. Ding, and J. Guo, Mesozoic and Cenozoic tectonic evolution of the Shiquanhe area of western Tibet, *Tectonics*, *22*(4), 1029, doi:10.1029/2001TC001332, 2003.

## 1. Introduction

[2] Studies of active geologic processes along the margins of the Tibetan plateau have been used to infer the dominant mechanisms of plateau evolution during the Cenozoic Indo-Asian collision. Large-magnitude shortening of supracrustal rocks within the Himalaya [*Coward and Butler*, 1985; *Schelling*, 1992; *Srivastava and Mitra*, 1994; *DeCelles et al.*, 1998, 2001] coupled with the scarcity of Cenozoic upper crustal shortening in southern Tibet [*Burg et al.*, 1983; *Allègre et al.*, 1984; *Burg and Chen*, 1984; *Coulon et al.*, 1986; *Murphy et al.*, 1997] imply Tibetan plateau formation by subduction [*Argand*, 1924; *Powell and Conaghan*, 1973] or lower crustal injection [*Zhao and Morgan*, 1987] of India beneath Tibet. Along the southwestern and northwestern margins of Tibet, >1000-km-long strike-slip faults (Figure 1) are proposed to have accommodated northward indentation of India by laterally extruding Tibet eastward [*Tapponnier et al.*, 1982; *Peltzer and Tapponnier*, 1988; *Avouac and Tapponnier*, 1993]. Northeastern Tibet exhibits active thrust faulting and development of large ''bathtub-like'' basins [*Métivier et al.*, 1998; *Meyer et al.*, 1998], and is bounded on its southern margin by the active left-slip Kunlun strike-slip fault (Figure 1) [*Kidd and Molnar*, 1988; *Van der Woerd et al.*, 1998]. These observations have been used to suggest plateau growth by crustal thickening and sedimentary basin infilling concomitant with oblique subduction of continental mantle [*Métivier et al.*, 1998; *Meyer et al.*, 1998; *Tapponnier et al.*, 2001]. Analysis of plateau topography, studies of Pliocene to Recent surface deformation in central eastern Tibet, and lack of significant Cenozoic foreland basinal

[1]Now at Department of Geosciences, University of Arizona, Tucson, Arizona, USA.

[2]Now at Department of Geosciences, University of Houston, Houston, Texas, USA.

[3]Also at Institute of Advanced Studies, Australian National University, Canberra ACT, Australia.


0278-7407/03/2001TC001332

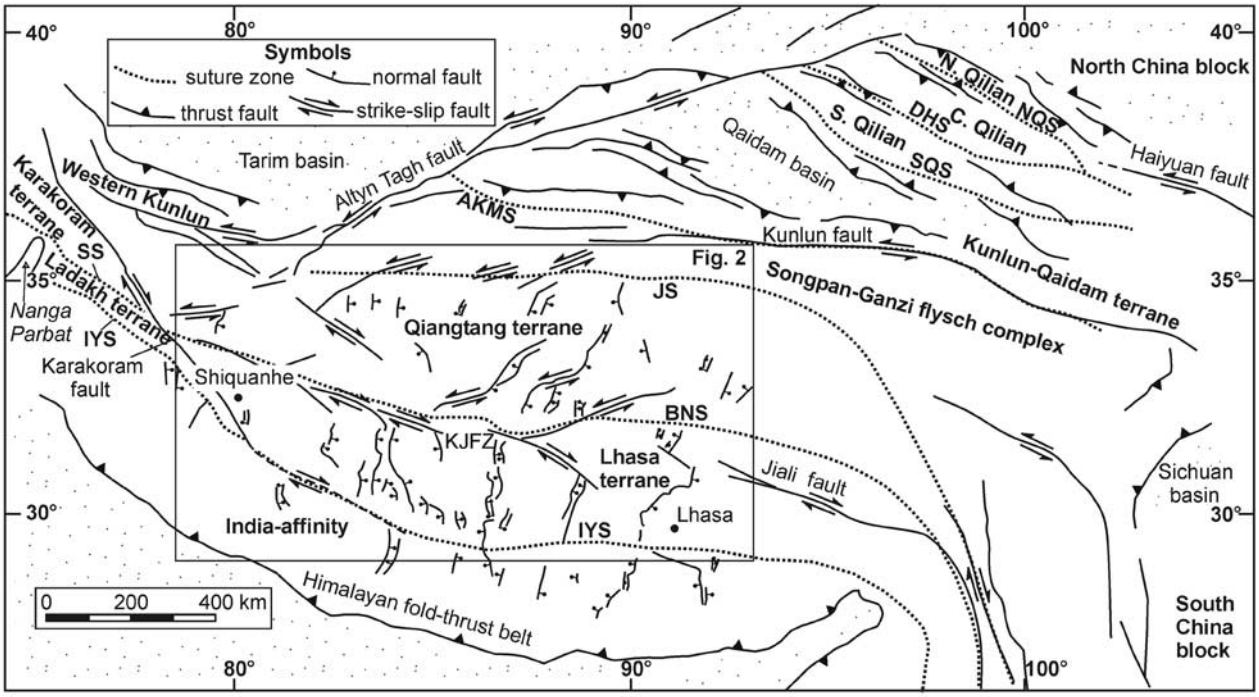


**Figure 1.** Tectonic map of Tibet showing major terranes, suture zones and active faults. From north to south, the sutures are the NQS, North Qilian; DHS, Danghe Nan Shan; SQS, South Qilian; AKMS, Anyimaqin-Kunlun-Muztagh; JS, Jinsha; BNS, Bangong-Nujiang; and IYS, Indus-Yalu. The Shyok suture (SS) is also shown, west of the Karakoram fault. The system of en echelon right-slip faults along the Bangong-Nujiang suture constitutes the Karakoram-Jiali fault zone (KJFZ) of *Armijo et al.* [1989].

strata along the eastern plateau margin highlight the important role of lower crustal flow in plateau growth [*Bird*, 1991; *Fielding et al.*, 1994; *Royden et al.*, 1997; *Clark and Royden*, 2000; *Kirby et al.*, 2000; *Shen et al.*, 2001].

[3] The extent to which active geologic processes observed along the margins of the Tibetan plateau can be used to infer how the plateau interior formed remains unclear. Active faults within the plateau are dominated by north to northeast striking normal faults and kinematically linked strike-slip faults [*Armijo et al.*, 1986, 1989; *Taylor et al.*, 2003; *Yin et al.*, 1999b; *Yin*, 2000], and could not have been responsible for producing the thick crust of Tibet. This observation emphasizes the potentially extreme spatial and temporal variability in plateau-forming processes, as well as the importance of constraining the style, timing, and slip magnitude of inactive fault systems in the interior of Tibet.

[4] Previous field studies have noted that Cenozoic upper crustal shortening in central Tibet is localized along Mesozoic oceanic suture zones and is relatively minor within the Lhasa and Qiangtang terranes [*Coulon et al.*, 1986; *Coward et al.*, 1988; *Matte et al.*, 1996; *Murphy et al.*, 1997; *Yin and Harrison*, 2000]. While these observations are inconsistent with distributed upper crustal shortening of Tibetan crust during the Indo-Asian collision [*Dewey and Burke*, 1973; *England and Houseman*, 1986], the possibility for large-magnitude intracontinental shortening along older suture zones remains to be tested [e.g., *Meyer et al.*, 1998; *Yin and Harrison*, 2000; *Tapponnier et al.*, 2001]. Additionally, it is uncertain to what extent the Tibetan crust was thickened prior to the Indo-Asian collision. Significant Cretaceous upper crustal shortening has been documented in southern Tibet [*Pan*, 1993; *Murphy et al.*, 1997]. Two end-member mechanisms for how the deeper crust may have accommodated this shortening are (1) homogenous crustal thickening, and (2) northward underthrusting of southern Tibet beneath central Tibet [*Murphy et al.*, 1997]. Constraining the relative importance of these processes, along with the total magnitude of Cretaceous shortening, is critical for estimating the crustal thicknesses of southern and central Tibet prior to the Indo-Asian collision.

[5] The Shiquanhe area (Figures 1 and 2) is an ideal locale to constrain the timing and relative importance of lateral extrusion, suture zone reactivation, and intra-terrane shortening in western Tibet. The Shiquanhe area exposes ophiolitic melange, upper Paleozoic-Mesozoic strata, Mesozoic granitoids, and Tertiary nonmarine strata and volcanic rocks [*Cheng and Xu*, 1986]. Based on reconnaissance-style studies, *Matte et al.* [1996] interpreted the ophiolitic melange to represent the remnants of a late Mesozoic suture zone that was reactivated during Late Cretaceous-Paleocene time. Both *Cheng and Xu* [1986] and *Matte et al.* [1996] suggested that Tertiary-Quaternary nonmarine basin fill occur in the footwall of north dipping thrusts located immediately north of the town of Shiquanhe. In contrast, *Ratschbacher et al.* [1994] inferred from structural analysis of serpentinite bodies that faults near Shi-

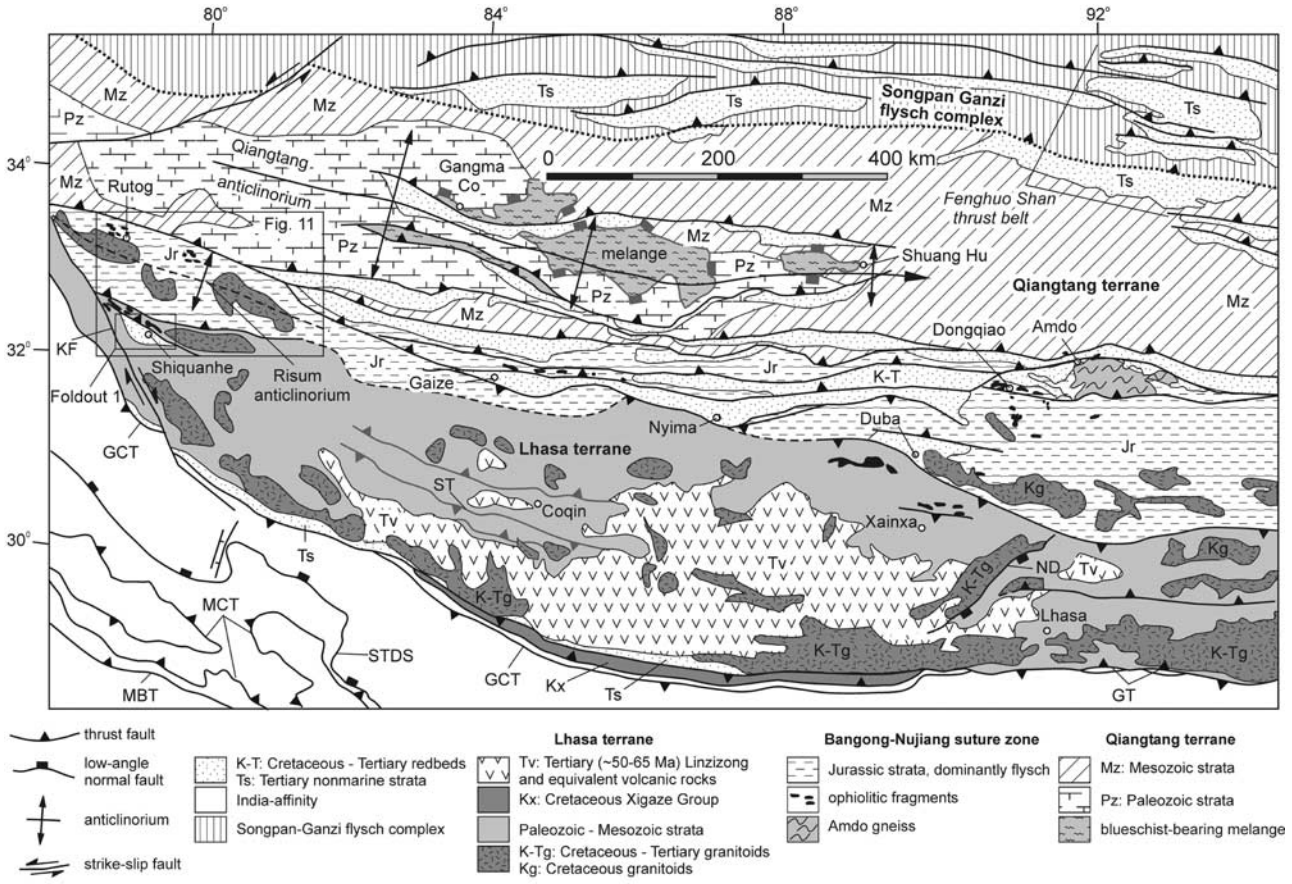


**Figure 2.** Tectonic map of southern and central Tibet. Tertiary thrust faults are shown by heavy black lines. Major Mesozoic faults are shown by heavy gray lines (Coqin thrust belt of *Murphy et al.* [1997] and early Mesozoic low-angle normal faults in the central Qiangtang terrane [*Kapp et al.*, 2000]). Map compiled from *Liu* [1988], *Kidd et al.* [1988], *Yin et al.* [1994], *Murphy et al.* [1997], and our unpublished mapping along the Bangong-Nujiang suture and in the Qiangtang terrane. Abbreviated faults are: GCT, Great Counter thrust; GT, Gangdese thrust; KF, Karakoram fault; MBT, Main Boundary Thrust; MCT, Main Central Thrust; ND, Nyainqentanghla detachment; ST, Shibaluo thrust; STDS, Southern Tibetan Detachment System.

quanhe constitute a major dextral strike-slip fault zone that transfers slip from the right-slip, Miocene-Recent Karakoram fault to north trending rifts in west central Tibet.

[6] We conducted mapping at a scale of 1:100,000 and geochronologic studies of the Shiquanhe area during 1997 and 1998. Our goals were to evaluate the tectonic significance of Shiquanhe ophiolitic melange and the extent to which major faults in the Shiquanhe area (1) transferred slip from the Karakoram fault, and (2) modified the Bangong-Nujiang suture zone following Late Jurassic-Early Cretaceous ocean closure. On the basis of our studies and interpretations of the regional geology, we make a first attempt at constructing a palinspastic restoration of Mesozoic-Cenozoic deformation in western Tibet.

## 2. Regional Geologic Background

[7] Tibet is an amalgamation of terranes that were accreted to the southern margin of Eurasia during Phanerozoic time [*Chang and Zheng*, 1973; *Allègre et al.*, 1984; *Dewey et al.*, 1988; *Hsü et al.*, 1995; *Yin and Harrison*, 2000]. From north to south, these terranes are the Qilian, Kunlun-Qaidam, Songpan-Ganzi flysch complex, Qiangtang, and Lhasa terranes (Figure 1). Terrane boundaries are defined by widely scattered belts of ophiolitic fragments and melanges. The Shiquanhe area lies within the westernmost extent of the Lhasa terrane in Tibet, exposes ophiolitic melange associated with the Bangong-Nujiang suture zone, and is located ~40 km northeast of the Karakoram fault zone.

### 2.1. Bangong-Nujiang Suture Zone

[8] The Bangong-Nujiang suture zone separates the Qiangtang terrane to the north from the Lhasa terrane to the south (Figure 1). It is characterized by a >1200-km-long east-west trending belt of widely scattered ophiolitic fragments that are associated with thick sequences of Jurassic flysch, melange, and volcanic rocks [*Wang et al.*, 1983; *Cheng and Xu*, 1987; *Yin et al.*, 1988] (Figure 2). The belt exhibits an anomalously large across-strike width, especially in far

western Tibet between Rutog and Shiquanhe (~100 km) and northwest of Lhasa between Xainza and Amdo (~200 km). It is debated whether the ophiolitic fragments represent remnants of (1) a single ophiolite sheet that was obducted southward from a north dipping subduction zone along the southern margin of the Qiangtang terrane [*Girardeau et al.*, 1984, 1985; *Coward et al.*, 1988], or (2) two or more different oceans that were separated by one or more intra-oceanic arc terranes [*Mei et al.*, 1981; *Srimal*, 1986; *Pearce and Deng*, 1988; *Hsü et al.*, 1995; *Matte et al.*, 1996; *Dunlap and Wysoczanski*, 2002]. Ophiolitic fragments southwest of Amdo (in the Dongqiao area, Figure 2) formed during the Jurassic [*Tang and Wang*, 1984] and were obducted at ~175 Ma [*Zhou et al.*, 1997], prior to deposition of unconformably overlying uppermost Jurassic-lowermost Cretaceous nonmarine to shallow marine strata [*Girardeau et al.*, 1984; *Tang and Wang*, 1984]. The more southerly ophiolitic fragments in the Shiquanhe and Xainza areas were obducted prior to deposition of unconformably overlying Aptian-Albian volcanic rocks and shallow marine limestones [*Girardeau et al.*, 1985; *Cheng and Xu*, 1987; *Matte et al.*, 1996].

[9] North of Shiquanhe, tectonic elements of the Bangong-Nujiang suture zone include the east-west trending, ~50-km-wide Risum anticlinorium and belt of ophiolitic melange near Rutog (Figure 2). The Risum anticlinorium (summary after *Matte et al.* [1996]) is characterized by Cretaceous strata along its limbs and a core of transposed, strongly cleaved Jurassic flyschoid slates. Locally, the southern limb of the anticlinorium is overturned, and Cretaceous strata exhibit a strong cleavage concordant with that in the Jurassic flysch. The southern limb is cut to the south by the north dipping Jaggang thrust. Jurassic strata in the core of the Risum anticlinorium are intruded by weakly deformed granitoid plutons, one of which is interpreted to be ~74 Ma based on a Rb/Sr age on biotite from hornfels in its contact aureole. $^{40}Ar/^{39}Ar$ and fission track thermochronologic studies suggest an episode of rapid cooling between 70 and 60 Ma, perhaps due to erosional denudation in response to growth of the Risum anticlinorium during this time. The melange near Rutog contains blocks of ophiolitic fragments, chert, and limestones that are Permo-Carboniferous and Aptian in age [*Matte et al.*, 1996], and is imbricated by south directed thrusts [*Ratschbacher et al.*, 1994]. Synkinematic muscovite from a south directed shear zone yielded a K-Ar age of 83 ± 4 Ma, and is interpreted to provide an estimate for the age of suture zone reactivation [*Ratschbacher et al.*, 1994]. The suture zone continued to accommodate north south shortening during the Indo-Asian collision, as Rutog melange is locally thrust southward over lower Tertiary red beds [*Cheng and Xu*, 1986]. In addition, Tertiary thrusts have been documented along-strike to the east near Gaize, Duba, and Amdo (Figure 2) [*Cheng and Xu*, 1986; *Coward et al.*, 1988; *Kidd et al.*, 1988; *Leeder et al.*, 1988; *Kapp et al.*, 1999].

### 2.2. Lhasa Terrane

[10] The Lhasa terrane is defined to lie between the Bangong-Nujiang suture zone to the north and the Indus-Yalu suture zone to the south (Figure 1) [*Chang and Zheng*, 1973; *Allègre et al.*, 1984; *Dewey et al.*, 1988]. The north south width of the Lhasa terrane decreases from east to west, being ~300 km wide at longitude 91°E near Lhasa and ~100 km wide at longitude 80°E near Shiquanhe. A surprising observation given its anomalously thick crust and high elevation, and its location just north of the indenting Indian continent, is the scarcity of basement exposures within southern Tibet (Figure 2) [*Liu*, 1988]. The Cambrian Amdo gneiss has been suggested to represent Lhasa terrane basement [*Xu et al.*, 1985; *Dewey et al.*, 1988]. However, given its complex structural setting within the Bangong-Nujiang suture zone (Figure 2) and its similar age to a block of high-grade gneiss within early Mesozoic melange of the central Qiangtang terrane [*Kapp et al.*, 2000], a Qiangtang affinity should not be ruled out.

[11] Paleozoic strata within the Lhasa terrane consist of a sequence of Ordovician to Permian, dominantly shallow marine strata [*Leeder et al.*, 1988; *Yin et al.*, 1988]. Upper Triassic strata are restricted primarily to southeastern Tibet, where they include limestone turbidites and volcanic sequences attributed to rifting of the Lhasa terrane from Gondwana [*Leeder et al.*, 1988; *Pearce and Mei*, 1988]. Jurassic interbedded sandstone, shale, limestone, and volcanic rocks lie unconformable on Triassic and older rocks of the Lhasa terrane and exhibit an increase in thickness from south to north [*Wang et al.*, 1983; *Cheng and Xu*, 1987; *Yin et al.*, 1988]. Lower Cretaceous shallow marine and nonmarine strata are widely exposed in the Lhasa terrane [*Leeder et al.*, 1988; *Yin et al.*, 1988; *Zhang*, 2000] and are commonly separated from underlying rocks by angular unconformities [*Kidd et al.*, 1988; *Liu*, 1988]. These Lower Cretaceous strata are proposed to have been deposited in either a back arc [*Zhang*, 2000], intra-arc [*Pan*, 1993], or foreland basin related to the Lhasa-Qiangtang collision [*Leeder et al.*, 1988; *Yin et al.*, 1994]. Development of a regional unconformity during Late Cretaceous time is evidenced by the widespread occurrence of weakly deformed volcanic sequences of early Tertiary age (Linzizong Formation; 65–50 Ma) (Figure 2) that overlie strongly deformed mid-Cretaceous strata [*Burg et al.*, 1983; *Allègre et al.*, 1984; *Burg and Chen*, 1984; *Coulon et al.*, 1986; *Pan*, 1993; *Murphy et al.*, 1997]. Tertiary nonmarine strata are scarce within the interior of the Lhasa terrane [*Liu*, 1988].

[12] Granitoids within the Lhasa terrane include the Cretaceous-Tertiary Gangdese (Transhimalaya) plutonic belt just north of the Indus-Yalu suture, and an Early Cretaceous belt within the northern Lhasa terrane [*Xu et al.*, 1985; *Harris et al.*, 1988, 1990]. Emplacement of the Gangdese batholith is attributed to northward subduction of Tethyan oceanic lithosphere beneath the southern margin of the Lhasa terrane [*Dewey and Bird*, 1970; *Chang and Zheng*, 1973; *Tapponnier et al.*, 1981; *Allègre et al.*, 1984]. The origin of granitoids in the northern Lhasa terrane is less clear; they are proposed to be related to shallow dipping northward subduction of Tethyan oceanic lithosphere [*Coulon et al.*, 1988] or crustal anatexis during either crustal thickening [*Xu et al.*, 1985] or lithospheric attenu-

ation [*Harris et al.*, 1990] following Lhasa-Qiangtang continental collision.

[13] The interior of the Lhasa terrane experienced significant upper crustal shortening during Cretaceous time. In the Coqin area (Figure 2), *Murphy et al.* [1997] documented >180 km of Cretaceous north south shortening. The mid-Cretaceous Takena Formation near Lhasa experienced ~40% shortening prior to deposition of overlying Linzizong volcanic rocks [*Pan*, 1993]. Minor Cenozoic upper crustal shortening is implied for large areas of the Lhasa terrane where weakly deformed lower Tertiary volcanic rocks are preserved [*Liu*, 1988; *Yin et al.*, 1994]. However, to the south, the Indus-Yalu suture zone was strongly modified by the Late Oligocene (30–23 Ma) north dipping Gangdese thrust system and the Miocene (19–10 Ma) south dipping Great Counter thrust system [*Yin et al.*, 1994; *Quidelleur et al.*, 1997; *Yin et al.*, 1999a; *Harrison et al.*, 2000].

### 2.3. Karakoram Fault and Kohistan-Karakoram Collision Belt

[14] The right-slip Karakoram fault extends >1000 km from the northern Pamirs to southwestern Tibet and cuts Tibetan terranes along their western margins (Figures 1 and 2). Correlating geology across the fault is difficult because the Kohistan-Karakoram belt to the west of the Karakoram fault records a significantly different geologic history (both prior to and during the Indo-Asian collision) and exposes deeper structural levels than the Tibetan orogen to the east [*Searle*, 1996a]. From south to north, the Kohistan-Karakoram collision belt consists of the Kohistan arc terrane, the Shyok suture zone, and the Karakoram terrane [see *Searle et al.*, 1999, and references therein]. The Kohistan arc terrane is a Cretaceous oceanic island arc complex that was superimposed by Andean-type magmatism of the Kohistan-Ladakh batholith, subsequent to collision with the Karakoram terrane along the Cretaceous (pre-75 Ma) Shyok suture zone and prior to India-Asia collision at ~65–50 Ma. The Karakoram terrane consists of an Ordovician to Early Cretaceous sedimentary belt to the north that is separated from the Karakoram high-grade metamorphic complex to the south by the Mesozoic-Cenozoic Karakoram batholith. Interpreting how the Lhasa terrane correlates with the Karakoram or the Kohistan-Ladakh terranes depends largely on the magnitude of slip along the Karakoram fault system [e.g., *Hodges*, 2000].

[15] Early total-slip estimates for the Karakoram fault were provided by offset of regional tectonic markers such as the Ladakh-Gangdese Batholith (~1000 km) [*Peltzer and Tapponnier*, 1988] and the Indus-Yalu suture zone (~200 km) [*Ratschbacher et al.*, 1994]. Detailed studies along the central portion of the Karakoram fault have suggested 150 to 120 km of separation [*Searle*, 1996b; *Searle et al.*, 1998], with slip initiating at ~17 Ma [*Dunlap et al.*, 1998]. This separation estimate suggests that the Kohistan-Ladakh batholith is correlative with the Gangdese batholith of southern Tibet, and that the Shyok suture is correlative with ophiolitic exposures near either Rutog [*Pan*, 1990; *Burtman and Molnar*, 1993; *Searle*, 1996b] or Shiquanhe [*Dunlap and Wysoczanski*, 2002]. In these correlations, there is no obvious counterpart to the Paleozoic and older rocks of the Lhasa terrane to the west of the Karakoram fault. In southwestern Tibet, the Karakoram fault offsets the ~13 Ma South Kailas thrust by ~66 km [*Murphy et al.*, 2000]. The recent estimates of offset and age of slip initiation are compatible if southward propagation of the Karakoram fault is considered [*Murphy et al.*, 2000].

## 3. Geology of the Shiquanhe Area

### 3.1. Rock Units

[16] Lithostratigraphic units mapped in the Shiquanhe area are summarized in Figure 3. Stratigraphic age assignments were made by correlating lithostratigraphy with biostratigraphic sections within or immediately adjacent to the study area [*Cheng and Xu*, 1987]. The oldest strata exposed are Permian and were divided into a lower unit (P1) and an upper unit (P2). Both units are disrupted internally by mesoscale faults and folds. P1 is >900 m thick and consists of interbedded arkosic sandstone, siltstone, shale, bluish-gray limestone and intraformational conglomerate. P2 consists of well-bedded, chert-nodule-bearing limestone, bedded chert, and sandstone. The limestones are sandy and contain abundant crinoid and coral fossils. P2 is the major cliff-forming unit immediately northeast of Shiquanhe. The contact between P1 and P2 is a slight angular unconformity.

[17] Jurassic strata (Jr) are exposed in the north part of the field area (Foldout 1). They consist of dark-colored interbedded graywacke, siltstone, shale, and intraformational conglomerate. The entire unit is tightly folded and the shales exhibit a slaty cleavage. We interpret the measured thickness of >5000 m for this sequence [*Cheng and Xu*, 1987] to represent a structural as opposed to a stratigraphic thickness due to the transposed nature of this unit.

[18] The most widespread strata in the Shiquanhe area are Lower Cretaceous. They are mapped as a single unit (K), but consist of distinct upper and lower parts (Figure 3). The lower part includes shallow marine and subordinate non-marine deposits. These deposits consist of volcaniclastic and volcanic rocks, fine-grained sandstone, siltstone, shale, limestone, and conglomerate, with the latter becoming more dominant near the top of the section. The volcanic rocks are variable in composition, and include green-colored pyroxene-bearing basalts, white tuffs, and red porphyritic andesites. The unit is internally deformed and the more thinly bedded rocks exhibit isoclinal folds and well-developed cleavage. The upper part of the Cretaceous unit consists largely of fossiliferous, orbitolinid- and rudist-bearing limestone of Aptian-Albian age [*Cheng and Xu*, 1987], bedded at the meter scale. The thickness of the lower part of the Cretaceous unit varies significantly in the field area. Although the contact is poorly exposed, map relationships suggest that Cretaceous strata unconformably overlie ophiolitic melange as previously suggested [*Cheng and Xu*, 1987; *Ratschbacher et al.*, 1994; *Matte et al.*, 1996]. The ophiolitic melange (oph) consists of strongly sheared serpentinized peridotites and subordinate mafic gabbro, chert, and blocks of red limestone.

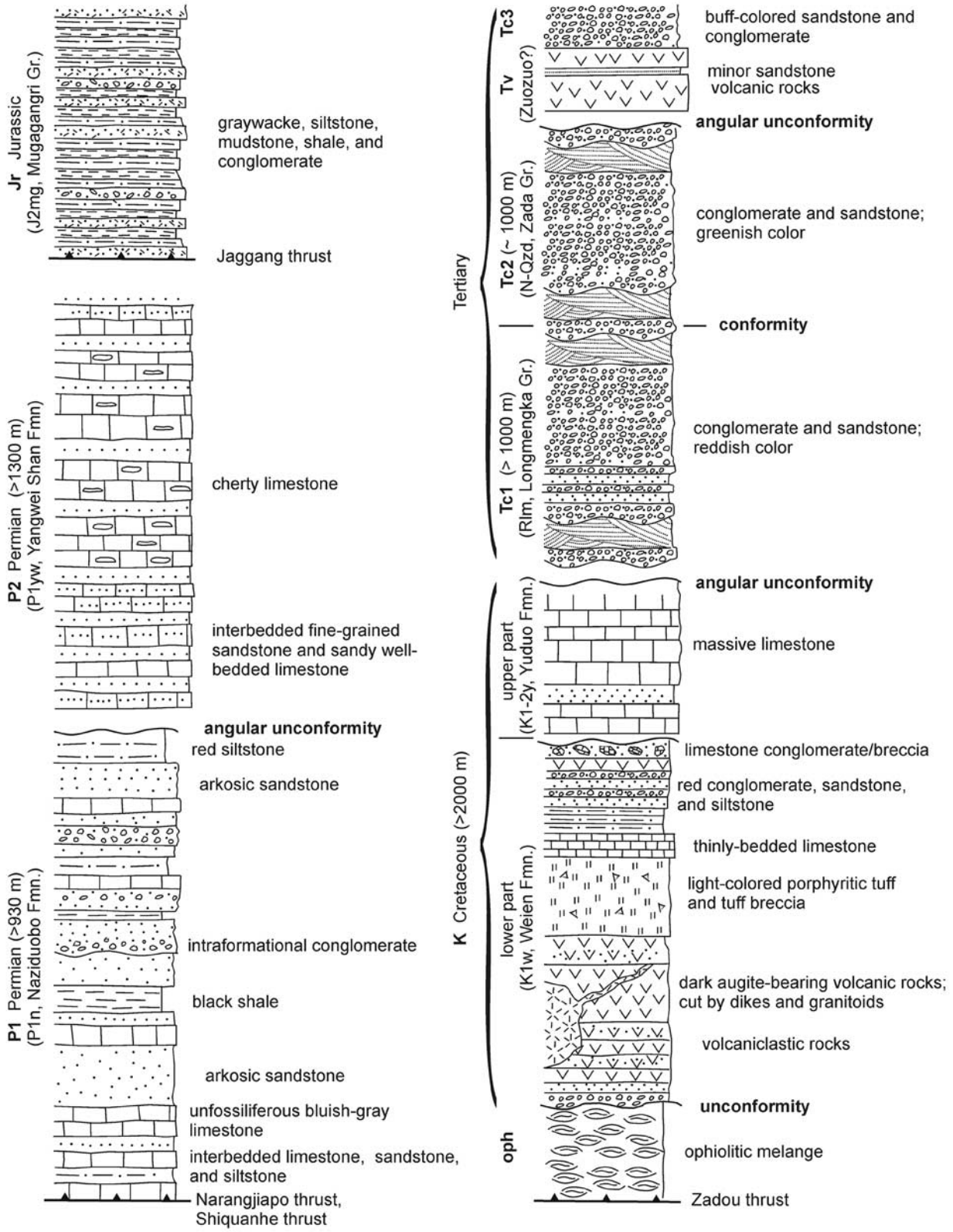


**Figure 3.** Lithostratigraphic column for the Shiquanhe area. In parentheses are correlative map units of *Cheng and Xu* [1987].

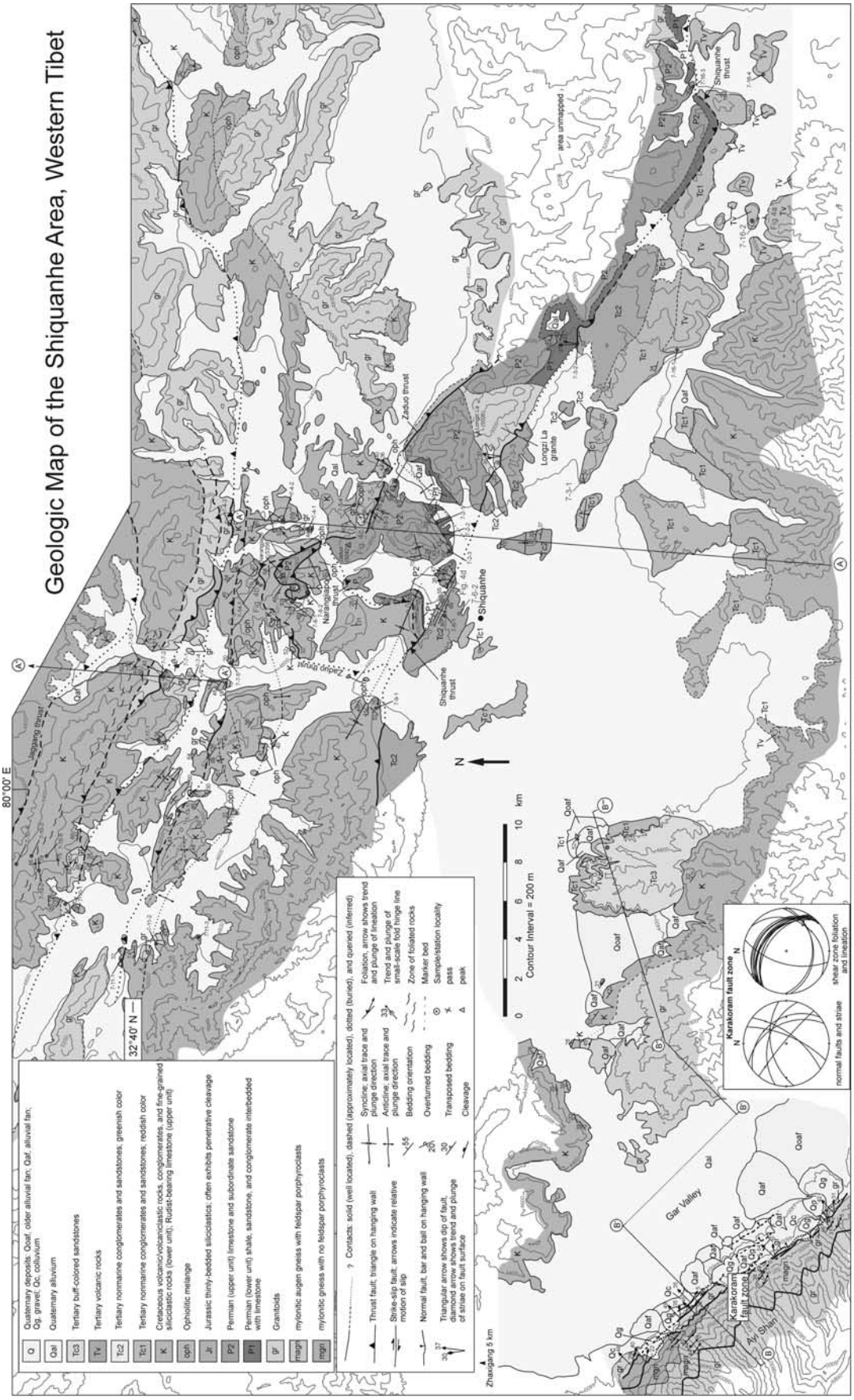


**Foldout 1.** Geologic map of the Shiquanhe area. Red arrows show where and in what direction photos in Figure 4 were taken. Sample localities discussed in the text are shown in red. Unmapped areas are in white. Cross-section lines A-A′-A″ and B-B′-B″-B are for Figures 5 and 6, respectively. Lower hemisphere, equal-area stereonets show structural data from the Karakoram fault zone. See enlarged version of this figure in the HTML.

[19] Exposures of folded Tertiary fluvial sandstone and conglomerate occur over a north south distance of ~18 km near Shiquanhe. Early workers divided Tertiary nonmarine rocks near Shiquanhe into three units [*Cheng and Xu*, 1987]. The lowest unit consists of sandstone and conglomerate, and was assigned to the Longmengka Group. The overlying middle unit consists of the Zuozuo volcanic rocks, one sample of which yielded a K-Ar whole rock age of ~38 Ma. The uppermost unit consists of gray sandstone and conglomerate and was correlated lithologically with the flat-lying Zada Group exposed ~100 km to the south, which is Middle Miocene or younger in age based on plant fossils [*Cheng and Xu*, 1987].

[20] We divided nonmarine strata near Shiquanhe into four units, which comprise a stratigraphy similar to that previously suggested by *Cheng and Xu* [1987]. The lowermost unit (Tc1) is red in color and consists of interbedded conglomerate and cross-bedded sandstone, with the conglomerate beds generally thicker (~2 m) than sandstone beds (5–30 cm). Orientations of trough-cross strata within the sandstones at locality 7-3-1 (Foldout 1) suggest a southeasterly paleocurrent direction (S10°E to S50°E). A conglomerate horizon at this locality contains clasts that consist of (1) variably colored volcanic rocks (47% of 105 clasts counted), (2) fine-grained granitoids (44%), and (3) sandstone, siltstone, and conglomerate (9%). Overlying the lowermost unit is another sequence of sandstone, siltstone, and conglomerate (Tc2). It is distinguished from Tc1 by its greenish color. Conglomerates within Tc2 contain clasts of limestone, chert, and serpentinized ultramafic material, in addition to volcanic rocks, siliciclastics, and granitoids. Orientations of imbricated pebbles at locality 7-6-2 indicate a paleocurrent direction toward the southwest. The contact between Tc1 and Tc2 is distinct at the map scale and appears to be conformable. In the southeastern portion of the field area, Tc1 is unconformably overlain by flat-lying volcanic rocks (Tv) (Figure 4a). The latter exhibit columnar jointing and are overlain by buff-colored sandstones and conglomerates (Tc3) southwest of Shiquanhe (Foldout 1).

[21] Exposures of granitoids (gr) are common in the Shiquanhe area, and generally become more abundant from west to east. The granitoids are mainly diorite to granodiorite in composition. Notable exceptions are (1) a muscovite-bearing granite that intrudes Permian strata to the east of Shiquanhe (here named the Longzi La granite after a nearby pass; Foldout 1), and (2) leucogranites which have been reported to intrude Cretaceous strata south of Shiquanhe [*Matte et al.*, 1996].

### 3.2. Structural Geology

[22] Our mapping of the Shiquanhe area (Foldout 1) documents previously unrecognized Late Cretaceous-early Tertiary folded thrust faults and a north dipping thrust system that soles into a decollement within ophiolitic melange. In addition, we show that the fault just north of Shiquanhe is a south directed thrust and that it cuts flat-lying volcanic rocks that lie unconformably on folded Tertiary nonmarine strata in its footwall. The trace of the Karakoram fault zone southwest of Shiquanhe is characterized by Quaternary-Recent, brittle, range-bounding normal right-slip faults that cut a right-slip mylonitic shear zone in their footwalls.

#### 3.2.1. Folded Faults

[23] The oldest fault mapped in the Shiquanhe area is the Narangjiapo thrust (here named after a 5356 m peak 10 km north of Shiquanhe; Foldout 1). It is regionally low angle, but is folded about variably oriented axes at the 100-meter to kilometer-scale. It juxtaposes Permian strata in the hanging wall, which are deformed by northeast-southwest trending folds, against ophiolitic melange and Cretaceous strata in the footwall (Foldout 1 and 4b). Regionally, the Narangjiapo thrust is subparallel to bedding in footwall Cretaceous strata and cuts the generally northwestward dipping Permian strata in the hanging wall. These relationships between fault orientation and hanging wall and footwall bedding constitute a hanging wall ramp on footwall-flat geometry. Based on the assumption that bedding orientation is related directly to displacement on the Narangjiapo thrust, we interpret this geometry to indicate northwest directed transport of the hanging wall over a southeast dipping thrust ramp (Figure 5) Tectonic burial of the thrust ramp in the footwall of the younger north dipping Shiquanhe thrust provides a simple explanation for why the inferred thrust ramp is not exposed at the surface. In contrast, if the Narangjiapo thrust sheet were derived from the north, a much more complex thrusting history would be required to explain the absence of a mapped root zone in the study area.

[24] The Narangjiapo thrust is cut by another folded thrust, the Zaduo thrust (here named after a 5042 m peak 8 km northeast of Shiquanhe; Foldout 1). It repeats the sequence of ophiolitic melange and unconformably overlying Cretaceous strata, and includes the thrust sheet of Permian strata in its footwall (Figures 4c and 5). The fault zone is characterized by an ~2-m-thick resistant ridge of orange-colored fault breccia and in some places a thick (>20 m) zone of strongly foliated and nearly completely serpentinized melange. At locality 7-5-1 (Foldout 1), the fault zone strikes N35°W, dips 40° to the northeast, and exhibits northeastward plunging slickenlines. Orientations of shear bands and asymmetric small-scale folds and serpentinite boudins within the fault zone suggest transport of the hanging wall to the south with respect to the footwall.

#### 3.2.2. Jaggang Thrust System

[25] Immediately to the north of the folded faults, Cretaceous strata and granitoid intrusions are repeated by three closely spaced (~2 km) north dipping thrusts (Foldout 1 and Figure 5). The granitoids are generally undeformed, except near thrust faults, where they are in some places strongly brecciated or weakly foliated. Just north of the imbricate thrust system is a subvertical, ~1-km-thick east-west trending zone of ductiley deformed greenschist-facies metavolcanic, calcareous, and metadioritic rocks. The tectonized rocks exhibit a strong foliation and either

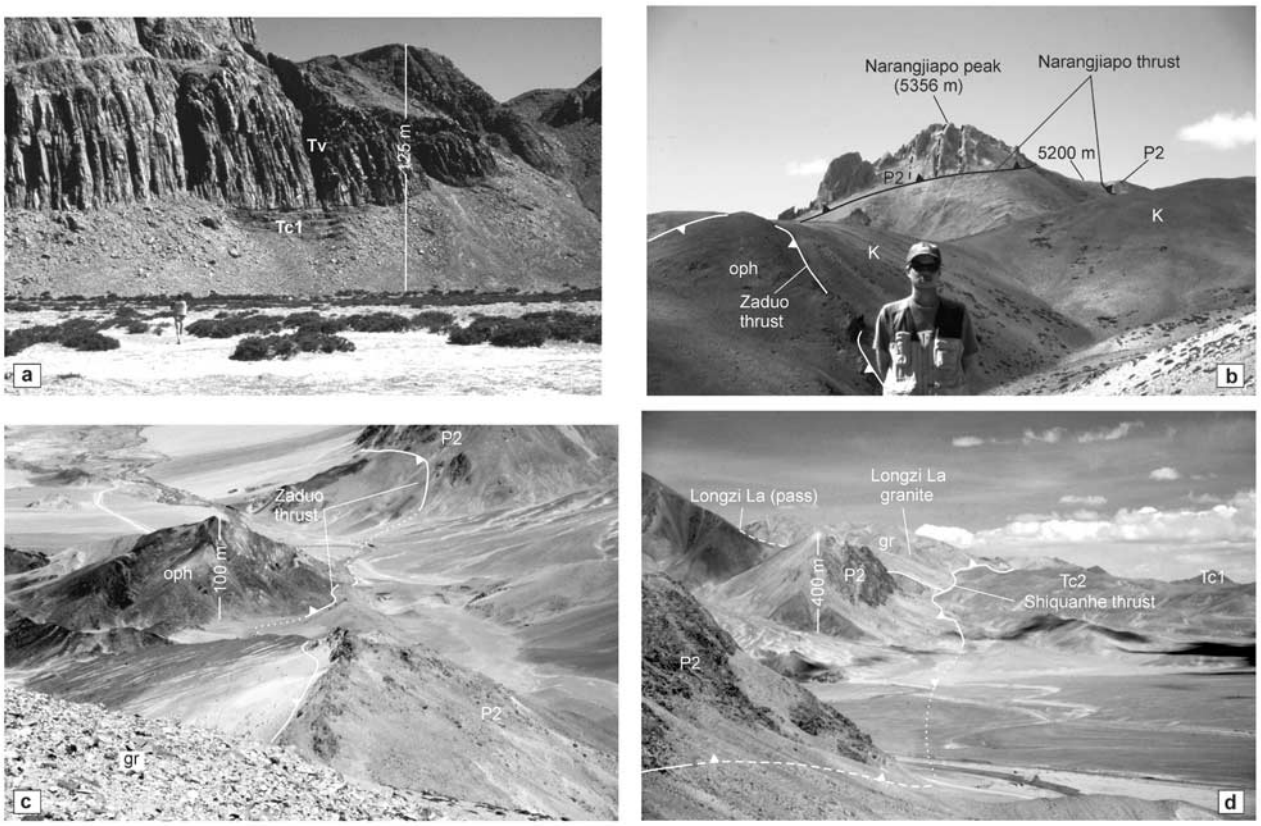


**Figure 4.** (a) View to north at flat-lying, columnar-jointed volcanic rocks overlying tilted red beds. The sample dated in this study (PK7-16-2) was collected from this exposure. (b) View of Narangjiapo and Zaduo thrusts looking toward southeast from near sample locality 7-14-1 (Foldout 1). The Narangjiapo thrust juxtaposes steeply dipping beds of Permian strata in the hanging wall against Cretaceous volcanic and volcaniclastic rocks in the footwall. Here, the Zaduo thrust is north dipping and places ophiolitic melange over Cretaceous rocks to the south. (c) Photo of Zaduo thrust taken from granite outcrop near locality 7-5-3 and looking toward the east-southeast. Here, it juxtaposes ophiolitic melange (dark-colored) in its hanging wall against Permian limestone and sandstone (gray) in its footwall. The fault zone is characterized by a resistant rib of orange fault breccia. (d) A view from ~2 km northeast of Shiquanhe (Foldout 1) toward the east-southeast along the trace of the Shiquanhe thrust. Here, the thrust juxtaposes Permian strata and the Longzi La granite in the hanging wall against green (Tc2) and red (Tc1) nonmarine basin fill in its footwall. See color version of this figure at back of this issue.

no stretching lineation or a weak, roughly subhorizontal mineral stretching lineation defined by quartz and calcite. Asymmetric boudinage, kink bands, and composite shear fabrics were observed locally, but do not suggest a consistent sense-of-shear. The deformation zone is characterized by a gradational decrease in strain toward its margins and is intruded by weakly foliated to undeformed granitoid sills. Pending additional kinematic studies, we tentatively interpret the subvertical deformation zone to be a result of north south pure-shear shortening that was localized during sill emplacement. The northernmost fault juxtaposes Jurassic flysch strata southward over Cretaceous strata (Foldout 1 and Figure 5), and is correlative to the Jaggang thrust of *Matte et al.* [1996]. Approximately 10 km northwest of the map area, a ~50-m-long by ~20-m-thick sliver of serpentinized melange was observed structurally beneath Jurassic strata in the hanging wall of the Jaggang thrust.

### 3.2.3. Shiquanhe Thrust

[26] The Shiquanhe thrust dips moderately to the north or northeast and places Permian and Cretaceous strata, the Longzi La granite, and ophiolitic melange in the hanging wall over deformed Tertiary fluvial strata and overlying flat-lying volcanic rocks in the footwall (Foldout 1 and Figures 4d and 5). In addition, the Shiquanhe thrust cuts both the Narangjiapo and Zaduo thrusts in its hanging wall. The Shiquanhe thrust surface is well exposed at several localities and north plunging slickenlines and

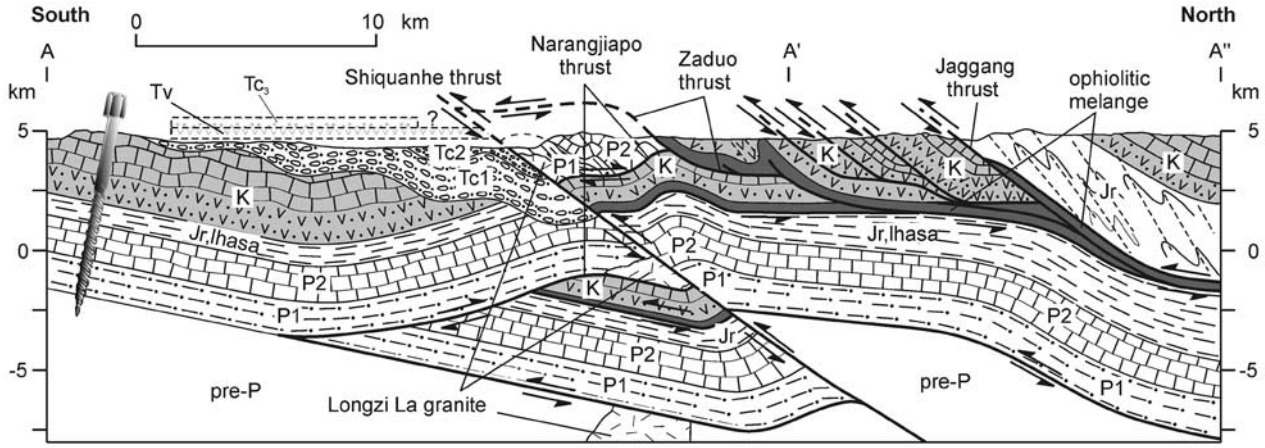


**Figure 5.** North-south cross section, Shiquanhe area. See Foldout 1 for explanation of abbreviations and location of A-A′-A″ section line, and text for the major assumptions that the cross section is based on. The dashed Tertiary units shown above the topographic profile (Tv and Tc3) are projected into the line of section. For simplicity, only the Longzi La granite is shown. Jr, lhasa are Jurassic strata of the Lhasa terrane. They are distinguished from the Jurassic strata (Jr) mapped in Foldout 1, which are interpreted to be allochthonous.

crystal fiber lineations along it indicate that it was south directed (Foldout 1).

#### 3.2.4. Karakoram Fault Zone

[27] A 16-km-long section of the Karakoram fault system was mapped (Foldout 1) and a cross section is shown in Figure 6. Mapping focused on three traverses through the basement rocks exposed along the Ayi Shan range front. The base of the Ayi Shan range front is characterized, structurally, by an ~2-km-wide zone of subparallel vertical to northeast dipping right-slip and normal-slip brittle faults. Range-front alluvial fans, glacial moraines, and colluvium are both cut by, and unconformably overlie, faults within this zone. At the range front, brittle normal-slip, right-slip, and right-slip normal faults dip between 54° and 40° to the northeast. Slip on these faults produced 500- to 1500-m-high triangular facets above the valley floor. The front 750 m of the range is characterized by a right-slip ductile shear zone of mylonitic orthogneisses. The intensity of shear strain decreases into the range. Stretching lineations within the shear zone trend consistently 140° and are horizontal (Foldout 1). Asymmetrically tailed feldspar augens, small-scale ductile shear zones, and S-C fabrics indicate right-lateral sense-of-shear.

## 4. U-Pb Geochronology and $^{40}Ar/^{39}Ar$ Thermochronology

[28] U-Pb ion microprobe studies and $^{40}Ar/^{39}Ar$ thermochronology on igneous rocks provide constraints on the timing of deformation in the Shiquanhe area. U-Pb single spot analyses on zircon were obtained using the CAMECA ims 1270 ion microprobe at UCLA. Zircon separates were obtained using standard mineral separation techniques. Grains were mounted in epoxy, polished, and coated with ~400 Å of Au. The relative sensitivity factor for U and Pb was obtained using a calibration curve defined by measurement of standard zircon AS-3 (1099.1 ± 0.5 Ma) [*Paces and Miller*, 1993]. Analyses were made using a 5–15 nA $O^-$ primary beam focused to a spot of ~20 μm diameter. The sample chamber was flooded with oxygen at a pressure of ~$3 \times 10^{-5}$ torr to enhance the yield of $Pb^+$ ionization [*Schuhmacher et al.*, 1994]. A mass resolving power of

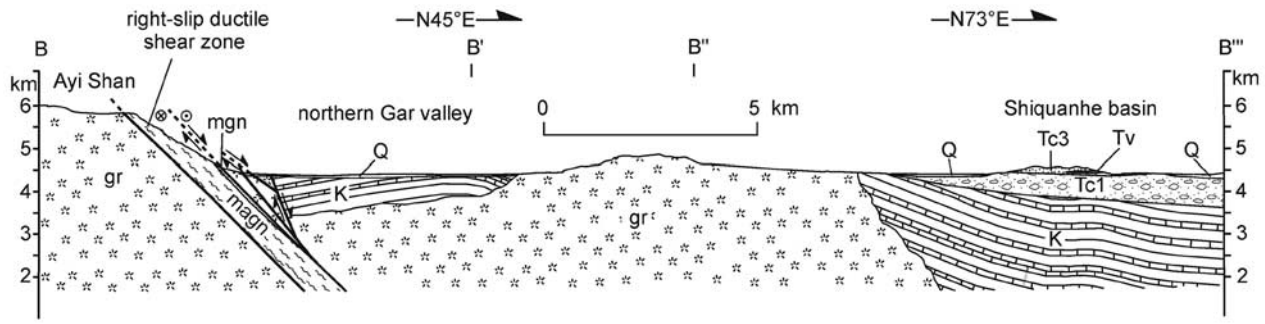


**Figure 6.** Cross section of the Karakoram fault zone. See Foldout 1 for explanation of abbreviations and location of B-B′-B″-B section line.

**Table 1.** Zircon U-Pb Isotopic Data for Sample 97-7-3-3bpk (Longzi La Granite)[a]

| | Isotopic Ratios | | | | | | | Apparent Ages ± 1σ | | |
|---|---|---|---|---|---|---|---|---|---|---|
| Spot[b] | $^{206}Pb^*/^{238}U$ | ±1 σ | $^{207}Pb^*/^{235}U$ | ±1 σ | $^{207}Pb^*/^{206}Pb^*$ | ±1 σ | $^{206}Pb^*$(%) | $^{206}Pb^*/^{238}U$ | $^{207}Pb^*/^{235}U$ | $^{207}Pb^*/^{206}Pb^*$ |
| 4,6,1 | 2.31E-02[c] | 5.47E-04 | 1.01E-01 | 4.19E-02 | 3.17E-02 | 1.27E-02 | 93.3 | 147 ± 3 | 98 ± 39 | negative |
| 4,4,1 | 2.39E-02 | 3.17E-04 | 1.47E-01 | 1.25E-02 | 4.46E-02 | 3.60E-03 | 98.5 | 152 ± 2 | 139 ± 11 | negative |
| 5,13,1 | 2.21E-02 | 4.06E-04 | 1.47E-01 | 1.22E-02 | 4.84E-02 | 3.71E-03 | 93.5 | 141 ± 3 | 139 ± 11 | 118 ± 181 |
| 5,11,1 | 2.23E-02 | 4.72E-04 | 1.41E-01 | 3.07E-02 | 4.59E-02 | 9.52E-03 | 93.9 | 142 ± 3 | 134 ± 27 | negative |
| 5,8,2 | 1.94E-02 | 2.59E-04 | 1.16E-01 | 1.13E-02 | 4.34E-02 | 3.97E-03 | 71.7 | 124 ± 2 | 112 ± 10 | negative |
| 5,4,1 | 2.36E-02 | 3.13E-04 | 1.51E-01 | 6.10E-03 | 4.63E-02 | 1.67E-03 | 99.0 | 150 ± 2 | 143 ± 5 | 14 ± 87 |
| 10,3,1 | 2.01E-02 | 6.60E-04 | 1.36E-01 | 1.05E-02 | 4.89E-02 | 3.18E-03 | 94.2 | 128 ± 4 | 129 ± 9 | 145 ± 153 |
| 10,19,1 | 2.01E-02 | 5.34E-04 | 1.25E-01 | 1.39E-02 | 4.50E-02 | 5.02E-03 | 97.4 | 128 ± 3 | 119 ± 12 | negative |
| 10,20,1 | 2.53E-02 | 3.45E-04 | 1.62E-01 | 1.59E-02 | 4.65E-02 | 4.31E-03 | 97.3 | 161 ± 2 | 153 ± 14 | 24 ± 222 |

[a]Asterisks refer to radiogenic Pb, corrected for common Pb with composition: $^{206}Pb/^{204}Pb = 18.49$; $^{207}Pb/^{204}Pb = 15.62$; $^{208}Pb/^{204}Pb = 37.63$, estimated from model of *Stacey and Kramers* [1975]. Negative apparent ages are due to reverse discordance.
[b]Spot identification. Numbers refer to row number, grain number, and spot number, respectively.
[c]Read 2.31E-02 as $2.31 \times 10^{-2}$.

~6000 was used to distinguish the $^{204}Pb$ peak from molecular interferences such as $^{176}Hf^{28}Si^+$ [*Compston et al.*, 1984]. Analyses were corrected for common Pb using measured $^{204}Pb$ and an isotopic composition estimated from the Pb evolution model of *Stacey and Kramers* [1975]. Additional details of the U-Pb analytical method have been described previously [*Quidelleur et al.*, 1997; *Harrison et al.*, 2000].

[29] Mineral separates for $^{40}Ar/^{39}Ar$ analysis were of high purity and irradiated at the Ford Reactor, University of Michigan. They were irradiated along with Fish Canyon sanidine [27.8 Ma; *Renne et al.*, 1994] flux monitors to determine J factors and $K_2SO_4$ and $CaF_2$ to determine correction factors for interfering neutron reactions. Samples were step-heated within a Ta crucible in a double-vacuum resistance furnace. $^{40}Ar/^{39}Ar$ isotopic measurements were performed using a VG 3600 mass spectrometer at UCLA. Stated errors for ages are at the 1σ level and do not include uncertainties in J factors or decay constants.

### 4.1. Longzi La Granite

[30] Nine euhedral zircons from a sample of Longzi La granite (97-7-3-3bpk) yield concordant U-Pb ion-microprobe spot ages that range between 124 and 161 Ma (Table 1 and Figure 7a). We interpret the weighted mean $^{206}Pb^*/^{238}U$ age of 126 ± 3 Ma (n = 3, 2σ) for the youngest population of zircons to be the best estimate for the crystallization age of the granite (Figure 7b), with the older ages being the result of variable mixing with an inherited component. The possibility that zircon in the granite crystallized at circa 161 Ma and experienced variable Pb loss is less likely, given the very high closure temperature for Pb diffusion in zircon [*Cherniak and Watson*, 2000], the undeformed nature of the Longzi La granite, and the low metamorphic grade of the host rock. In either interpretation, the Longzi La granite is older than the youngest strata that occur in the footwall of the Narangjiapo thrust (Albian), and therefore should be cut by the Narangjiapo thrust at depth (Figure 5).

[31] We conducted a $^{40}Ar/^{39}Ar$ step-heating experiment on K-feldspar to constrain the thermal history of the Longzi La granite subsequent to crystallization. The age spectrum was corrected for chlorine-correlated excess Ar ($^{40}Ar_E$) by conducting isothermal duplicates in the step-heating schedule at temperatures between 450 and 800°C ($^{40}Ar_E/Cl = 8.22 \pm 0.08 \times 10^{-5}$; see *Harrison et al.* [1994]). The chlorine-corrected age spectrum yields apparent ages that range from ~70 Ma during the initial heating

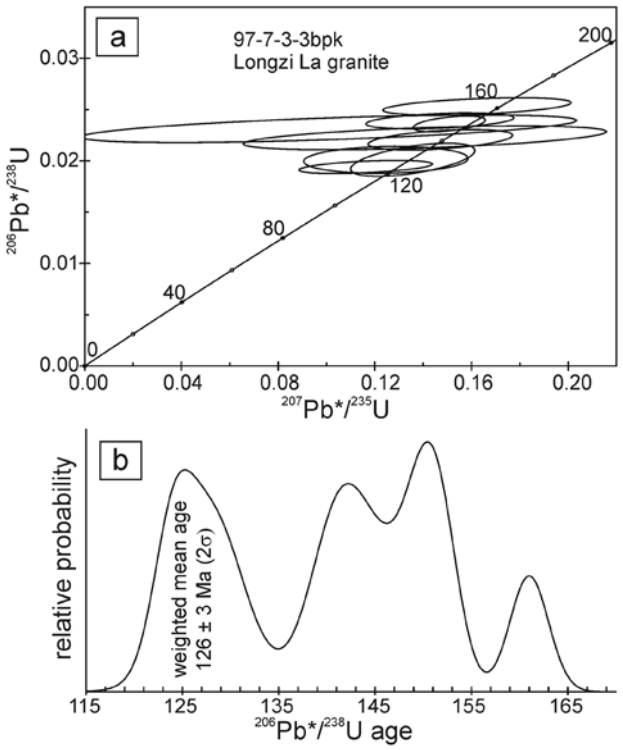


**Figure 7.** (a) U-Pb concordia plot showing results of single spot ion-microprobe analyses on zircon from the Longzi La granite. Sample was collected from locality 7-3-3 shown in Foldout 1. Error ellipses are 2 σ. (b) Curve showing relative probability versus $^{206}Pb^*/^{238}U$ age and the weighted mean age of the youngest population of zircons, which is interpreted to be the best estimate for the crystallization age.

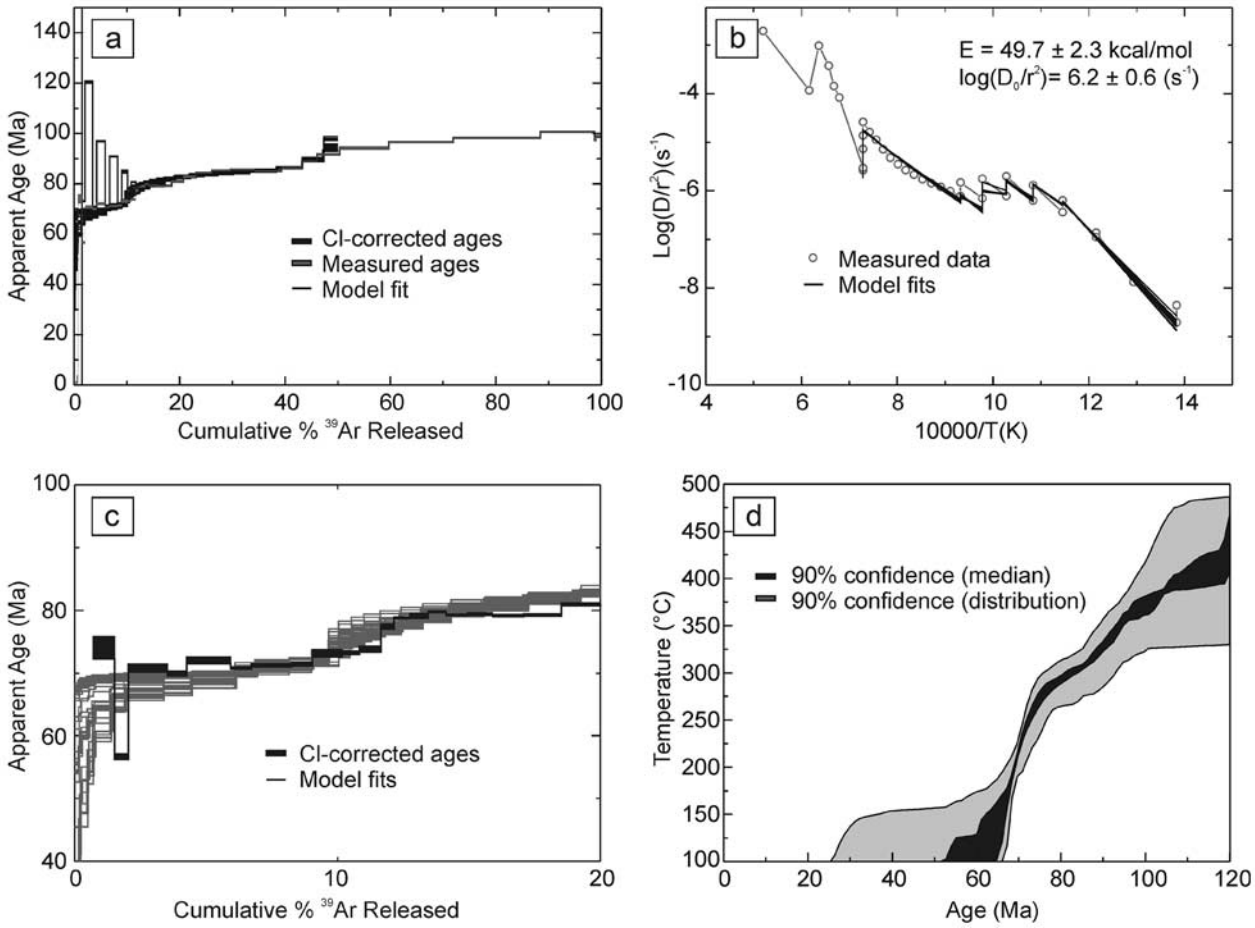


**Figure 8.** $^{40}Ar/^{39}Ar$ step-heating and multi-diffusion domain modeling results for K-feldspar separated from the Longzi La granite (sample 97-7-3-3bpk collected from locality 7-3-3 shown on Foldout 1). (a) Age spectrum. (b) Arrhenius plot. Initial heating steps (T < 600°C) yield a linear array with a slope that is proportional to the activation energy (E) and an upper intercept equal to log ($D_o/r_o^2$). (c) Close-up of age spectrum showing the first 20% $^{39}Ar$ released. (d) Model thermal history.

steps to ~100 Ma during the final steps (Figure 8a; Table 2). Portions of the age spectrum that were unaffected by low-temperature $^{40}Ar_E$ and obtained prior to melting at 1100°C (between 12% and 50% cumulative $^{39}Ar$ released) were cross-correlated with the corresponding log($r/r_o$) plot, yielding a correlation coefficient of 0.8 [*Lovera et al.*, 2002]. This value is a measure of the extent to which $^{39}Ar$ release from the K-feldspar sample at laboratory (during step-heating) and geologic timescales can be explained by a single volume diffusion process. A correlation coefficient of 0.8 is considered sufficient, although near the lower cutoff, for application of the multi-diffusion domain (MDD) model [*Lovera et al.*, 1989] and methods recently described [*Lovera et al.*, 1997; *Quidelleur et al.*, 1997; *Harrison et al.*, 2000] to extract useful thermal history information. Monotonic thermal histories obtained using MDD modeling provide reasonable fits to the age spectrum and the corresponding Arrhenius plot (Figure 8). The results suggest slow cooling between 75 and 100 Ma, followed by an episode of accelerated cooling from ~275°C to ~150°C between 75 and 65 Ma. We attribute rapid cooling to erosional denudation in response to regional thrust-related crustal thickening for two reasons. First, granitoids just south of Rutog experienced a similar thermal history of rapid cooling between 70 and 60 Ma [*Matte et al.*, 1996]. Second, the widely observed relationship of weakly deformed Paleocene-Eocene volcanic rocks lying unconformable on strongly deformed mid-Cretaceous strata provide unambiguous evidence for significant regional shortening and erosional denudation of southern Tibet during Late Cretaceous-earliest Tertiary time.

### 4.2. Age of Volcanic Rocks (Tv)

[32] The flat-lying volcanic rocks (Tv) provide an opportunity to place a younger bound on the age of Tertiary strata that they unconformably overlie (Foldout 1 and Figures 4b and 5). Argon isotopic measurements on biotite separated from the volcanic rocks (sample 97-7-16-2pk) yield a flat $^{40}Ar/^{39}Ar$ apparent age spectrum with a total gas age of 22.5 ± 0.1 Ma (1σ) and an inverse isochron age of

**Table 2.** Argon Isotopic Results[a]

| Step | T, °C | t, m | $^{40}Ar/^{39}Ar$[b] | $^{38}Ar/^{39}Ar$[b] | $^{37}Ar/^{39}Ar$[b] | $^{36}Ar/^{39}Ar$[b] | $^{39}Ar_K$, mol[c] | $\Sigma^{39}Ar_K$, % | $^{40}Ar^*$, %[d] | $^{40}Ar^*/Ar_K$[e] | $\pm\sigma_{40/39}$ | Age±1σ, Ma[f] | $^{39}Ar_K/^{40}Ar$[g] | $\pm\sigma_{39/40}$ | $^{36}Ar/^{40}Ar$[g] | $\pm\sigma_{36/40}$ |
|---|---|---|---|---|---|---|---|---|---|---|---|---|---|---|---|---|
| ***97-7-3-3bpk*** *K-Feldspar, Longzi La Granite (J = 0.007378) Total Gas Age = 94.2 ± 0.2 Ma (1σ) Irradiation Shipment: UM96T1* | | | | | | | | | | | | | | | | |
| 1 | 450 | 16 | 73.00 | 5.33E-01[h] | 0.0615 | 9.83E-02 | 9.93E-15 | 0.2 | 60.1 | 43.94 | 0.30 | 506.6 ± 4.2 | 1.38E-02 | 4.97E-05 | 1.34E-03 | 8.75E-06 |
| 2 | 450 | 24 | 18.32 | 1.36E-01 | 0.0324 | 3.57E-02 | 2.89E-15 | 0.3 | 41.9 | 7.73 | 0.20 | 100.1 ± 2.8 | 5.80E-02 | 4.58E-04 | 1.87E-03 | 4.34E-05 |
| 3 | 500 | 16 | 33.66 | 1.13E-01 | 0.0214 | 3.33E-02 | 9.98E-15 | 0.5 | 70.7 | 23.81 | 0.09 | 292.0 ± 1.5 | 3.00E-02 | 6.75E-05 | 9.67E-04 | 7.09E-06 |
| 4 | 500 | 21 | 8.79 | 3.76E-02 | 0.0187 | 8.82E-03 | 7.33E-15 | 0.7 | 69.7 | 6.16 | 0.06 | 80.2 ± 0.8 | 1.20E-01 | 6.00E-04 | 8.89E-04 | 2.83E-05 |
| 5 | 550 | 17 | 23.48 | 6.14E-02 | 0.0162 | 2.17E-02 | 3.44E-14 | 1.5 | 72.5 | 17.04 | 0.05 | 213.7 ± 0.9 | 4.28E-02 | 5.18E-05 | 9.17E-04 | 6.21E-06 |
| 6 | 550 | 22 | 6.44 | 1.79E-02 | 0.0292 | 2.75E-03 | 2.26E-14 | 2.0 | 86.8 | 5.61 | 0.02 | 73.1 ± 0.3 | 1.59E-01 | 3.53E-04 | 3.65E-04 | 1.06E-05 |
| 7 | 600 | 17 | 12.34 | 2.98E-02 | 0.0460 | 1.00E-02 | 6.35E-14 | 3.5 | 75.8 | 9.36 | 0.03 | 120.5 ± 0.6 | 8.15E-02 | 1.38E-04 | 8.02E-04 | 6.64E-06 |
| 8 | 600 | 21 | 5.95 | 1.29E-02 | 0.0453 | 1.69E-03 | 3.19E-14 | 4.3 | 91.1 | 5.43 | 0.01 | 70.9 ± 0.3 | 1.72E-01 | 4.27E-04 | 2.28E-04 | 8.36E-06 |
| 9 | 650 | 17 | 9.61 | 2.14E-02 | 0.0199 | 7.14E-03 | 7.14E-14 | 5.9 | 77.7 | 7.48 | 0.02 | 96.9 ± 0.3 | 1.05E-01 | 1.20E-04 | 7.33E-04 | 4.60E-06 |
| 10 | 650 | 21 | 6.06 | 1.28E-02 | 0.0117 | 1.94E-03 | 3.39E-14 | 6.7 | 90.0 | 5.46 | 0.02 | 71.3 ± 0.3 | 1.68E-01 | 3.96E-04 | 2.75E-04 | 8.81E-06 |
| 11 | 700 | 15 | 8.92 | 1.96E-02 | 0.0093 | 6.43E-03 | 6.54E-14 | 8.2 | 78.4 | 7.00 | 0.01 | 90.8 ± 0.3 | 1.13E-01 | 7.63E-05 | 7.09E-04 | 4.58E-06 |
| 12 | 700 | 23 | 6.09 | 1.29E-02 | 0.0088 | 1.82E-03 | 3.40E-14 | 9.0 | 90.6 | 5.53 | 0.01 | 72.2 ± 0.3 | 1.67E-01 | 3.06E-04 | 2.54E-04 | 8.38E-06 |
| 13 | 750 | 16 | 8.18 | 1.69E-02 | 0.0091 | 5.52E-03 | 4.85E-14 | 10.2 | 79.7 | 6.52 | 0.04 | 84.8 ± 0.8 | 1.24E-01 | 6.16E-04 | 6.56E-04 | 6.29E-06 |
| 14 | 750 | 26 | 6.39 | 1.31E-02 | 0.0091 | 2.23E-03 | 2.84E-14 | 10.8 | 89.1 | 5.70 | 0.02 | 74.4 ± 0.3 | 1.60E-01 | 3.51E-04 | 2.89E-04 | 1.05E-05 |
| 15 | 800 | 16 | 7.51 | 1.52E-02 | 0.0088 | 4.37E-03 | 3.49E-14 | 11.6 | 82.4 | 6.20 | 0.02 | 80.7 ± 0.3 | 1.35E-01 | 2.24E-04 | 5.50E-04 | 8.38E-06 |
| 16 | 800 | 20 | 6.65 | 1.27E-02 | 0.0079 | 2.33E-03 | 2.14E-14 | 12.1 | 89.0 | 5.94 | 0.04 | 77.4 ± 0.6 | 1.54E-01 | 7.29E-04 | 2.86E-04 | 1.39E-05 |
| 17 | 825 | 20 | 6.65 | 1.30E-02 | 0.0080 | 1.96E-03 | 2.59E-14 | 12.7 | 90.7 | 6.05 | 0.01 | 78.8 ± 0.3 | 1.54E-01 | 3.20E-04 | 2.35E-04 | 8.96E-06 |
| 18 | 850 | 20 | 6.66 | 1.29E-02 | 0.0083 | 1.91E-03 | 2.98E-14 | 13.4 | 91.0 | 6.07 | 0.03 | 79.1 ± 0.6 | 1.53E-01 | 6.49E-04 | 2.40E-04 | 1.14E-05 |
| 19 | 875 | 17 | 6.77 | 1.29E-02 | 0.0093 | 2.08E-03 | 2.91E-14 | 14.1 | 90.4 | 6.13 | 0.01 | 79.8 ± 0.3 | 1.51E-01 | 2.82E-04 | 2.60E-04 | 7.32E-06 |
| 20 | 900 | 18 | 6.73 | 1.29E-02 | 0.0082 | 2.10E-03 | 3.51E-14 | 14.9 | 90.3 | 6.09 | 0.01 | 79.3 ± 0.3 | 1.51E-01 | 2.50E-04 | 2.72E-04 | 6.23E-06 |
| 21 | 925 | 18 | 6.89 | 1.33E-02 | 0.0072 | 2.60E-03 | 4.11E-14 | 15.9 | 88.4 | 6.10 | 0.02 | 79.4 ± 0.3 | 1.47E-01 | 2.51E-04 | 3.46E-04 | 7.32E-06 |
| 22 | 950 | 19 | 7.06 | 1.43E-02 | 0.0065 | 3.23E-03 | 5.04E-14 | 17.1 | 86.0 | 6.08 | 0.02 | 79.1 ± 0.3 | 1.43E-01 | 1.34E-04 | 4.34E-04 | 8.64E-06 |
| 23 | 975 | 19 | 7.35 | 1.53E-02 | 0.0056 | 4.20E-03 | 6.20E-14 | 18.5 | 82.7 | 6.08 | 0.02 | 79.2 ± 0.3 | 1.38E-01 | 2.86E-04 | 5.47E-04 | 5.81E-06 |
| 24 | 1000 | 24 | 7.74 | 1.67E-02 | 0.0045 | 5.07E-03 | 9.56E-14 | 20.7 | 80.3 | 6.22 | 0.02 | 80.9 ± 0.3 | 1.30E-01 | 1.23E-04 | 6.44E-04 | 8.29E-06 |
| 25 | 1025 | 19 | 8.06 | 1.79E-02 | 0.0040 | 5.65E-03 | 1.02E-13 | 23.1 | 78.9 | 6.36 | 0.03 | 82.8 ± 0.5 | 1.25E-01 | 3.80E-04 | 6.94E-04 | 5.19E-06 |
| 26 | 1050 | 17 | 8.07 | 1.83E-02 | 0.0042 | 5.28E-03 | 1.28E-13 | 26.1 | 80.3 | 6.49 | 0.01 | 84.3 ± 0.3 | 1.25E-01 | 7.26E-05 | 6.48E-04 | 3.78E-06 |
| 27 | 1075 | 16 | 7.92 | 1.79E-02 | 0.0038 | 4.55E-03 | 1.53E-13 | 29.7 | 82.7 | 6.55 | 0.01 | 85.2 ± 0.3 | 1.27E-01 | 1.02E-04 | 5.69E-04 | 4.56E-06 |
| 28 | 1100 | 15 | 7.76 | 1.78E-02 | 0.0043 | 3.89E-03 | 2.00E-13 | 34.3 | 84.8 | 6.59 | 0.01 | 85.6 ± 0.3 | 1.30E-01 | 1.10E-04 | 4.97E-04 | 4.44E-06 |
| 29 | 1100 | 35 | 7.37 | 1.68E-02 | 0.0049 | 2.73E-03 | 2.14E-13 | 39.3 | 88.6 | 6.54 | 0.01 | 85.0 ± 0.3 | 1.36E-01 | 1.01E-04 | 3.66E-04 | 3.75E-06 |
| 30 | 1100 | 60 | 7.33 | 1.65E-02 | 0.0043 | 2.20E-03 | 1.72E-13 | 43.3 | 90.7 | 6.65 | 0.01 | 86.4 ± 0.3 | 1.37E-01 | 1.84E-04 | 2.94E-04 | 3.70E-06 |
| 31 | 1100 | 120 | 7.59 | 1.69E-02 | 0.0037 | 2.40E-03 | 1.16E-13 | 46.0 | 90.3 | 6.86 | 0.01 | 89.1 ± 0.3 | 1.33E-01 | 1.15E-04 | 3.06E-04 | 2.98E-06 |
| 32 | 1100 | 181 | 8.03 | 1.79E-02 | 0.0030 | 3.16E-03 | 1.84E-13 | 50.3 | 88.0 | 7.07 | 0.01 | 91.7 ± 0.3 | 1.25E-01 | 1.88E-04 | 3.89E-04 | 3.40E-06 |
| 33 | 1200 | 17 | 8.11 | 1.94E-02 | 0.0030 | 2.79E-03 | 4.01E-13 | 59.7 | 89.5 | 7.26 | 0.03 | 94.2 ± 0.6 | 1.24E-01 | 4.70E-04 | 3.42E-04 | 5.60E-06 |
| 34 | 1225 | 17 | 8.29 | 1.93E-02 | 0.0013 | 2.75E-03 | 5.23E-13 | 71.9 | 89.9 | 7.45 | 0.01 | 96.6 ± 0.3 | 1.21E-01 | 1.61E-04 | 3.30E-04 | 3.28E-06 |
| 35 | 1250 | 16 | 8.40 | 1.96E-02 | 0.0009 | 2.68E-03 | 7.08E-13 | 88.4 | 90.2 | 7.58 | 0.01 | 98.2 ± 0.3 | 1.19E-01 | 7.35E-05 | 3.19E-04 | 4.24E-06 |
| 36 | 1300 | 15 | 8.68 | 1.89E-02 | 0.0004 | 3.02E-03 | 4.40E-13 | 98.7 | 89.4 | 7.77 | 0.01 | 100.5 ± 0.3 | 1.16E-01 | 6.61E-05 | 3.46E-04 | 2.70E-06 |
| 37 | 1350 | 16 | 10.26 | 1.98E-02 | 0.0018 | 9.04E-03 | 1.38E-14 | 99.0 | 73.5 | 7.56 | 0.06 | 97.9 ± 0.7 | 9.99E-02 | 2.35E-04 | 8.29E-04 | 1.99E-05 |
| 38 | 1650 | 16 | 9.93 | 1.95E-02 | 0.0008 | 7.69E-03 | 4.34E-14 | 100 | 76.8 | 7.63 | 0.03 | 98.8 ± 0.5 | 1.02E-01 | 2.62E-04 | 7.58E-04 | 3.97E-06 |

**Table 2.** (continued)

| Step | T, °C | t, m | $^{40}Ar/^{39}Ar^b$ | $^{38}Ar/^{39}Ar^b$ | $^{37}Ar/^{39}Ar^b$ | $^{36}Ar/^{39}Ar^b$ | $^{39}Ar_K$, mol$^c$ | $\Sigma^{39}Ar_K$, % | $^{40}Ar^*$, %$^d$ | $^{40}Ar^*/Ar_K{}^e$ | $\pm\sigma_{40/39}$ | Age±1σ, Ma$^f$ | $^{39}Ar_K/^{40}Ar^g$ | $\pm\sigma_{39/40}$ | $^{36}Ar/^{40}Ar^g$ | $\pm\sigma_{36/40}$ |
|---|---|---|---|---|---|---|---|---|---|---|---|---|---|---|---|---|
| | | | | | | | | | | | | | | | | |
| | | | | | | | | | | | | | | | | |
| | | | | | | | | | | | | | | | | |
| | | | | | | | | | | | | | | | | |
| | | | | | | | | | | | | | | | | |
| | | | | | | | | | | | | | | | | |
| | | | | | | | | | | | | | | | | |
| | | | | | | | | | | | | | | | | |
| | | | | | | | | | | | | | | | | |

***97-7-16-2pk*** *Biotite, Volcanic (J = 0.007057, weight = 5.2 mg) Total Gas Age = 22.5 ± 0.1 Ma (1σ) Irradiation Shipment: UM92T1*

| | | | | | | | | | | | | | | | | |
|---|---|---|---|---|---|---|---|---|---|---|---|---|---|---|---|---|
| 1 | 500 | 30 | 17.47 | 5.87E-02 | 0.0062 | 5.53E-02 | 3.80E-15 | 0.4 | 6.1 | 1.11 | 0.15 | 14.1 ± 1.9 | 5.73E-02 | 1.52E-04 | 3.17E-03 | 2.86E-05 |
| 2 | 650 | 21 | 7.01 | 6.60E-02 | 0.0177 | 1.76E-02 | 2.90E-14 | 3.4 | 25.2 | 1.78 | 0.02 | 22.6 ± 0.3 | 1.43E-01 | 1.62E-04 | 2.52E-03 | 1.01E-05 |
| 3 | 730 | 21 | 2.80 | 6.71E-02 | 0.0002 | 3.30E-03 | 2.21E-13 | 26.4 | 64.1 | 1.80 | 0.01 | 22.8 ± 0.1 | 3.60E-01 | 2.18E-04 | 1.19E-03 | 8.46E-06 |
| 4 | 780 | 20 | 2.31 | 6.43E-02 | 0.0000 | 1.68E-03 | 1.67E-13 | 43.8 | 76.9 | 1.78 | 0.00 | 22.6 ± 0.05 | 4.38E-01 | 5.13E-04 | 7.38E-04 | 5.42E-06 |
| 5 | 820 | 20 | 2.32 | 6.30E-02 | 0.0000 | 1.76E-03 | 1.37E-13 | 58.1 | 75.9 | 1.77 | 0.00 | 22.4 ± 0.05 | 4.36E-01 | 4.92E-04 | 7.69E-04 | 3.59E-06 |
| 6 | 860 | 20 | 3.45 | 6.28E-02 | 0.0000 | 5.98E-03 | 4.12E-14 | 62.4 | 47.2 | 1.65 | 0.02 | 20.9 ± 0.3 | 2.92E-01 | 4.37E-04 | 1.75E-03 | 2.22E-05 |
| 7 | 950 | 20 | 3.65 | 6.88E-02 | 0.0011 | 6.44E-03 | 6.66E-14 | 69.3 | 46.8 | 1.72 | 0.02 | 21.8 ± 0.2 | 2.76E-01 | 2.37E-04 | 1.78E-03 | 1.38E-05 |
| 8 | 1150 | 20 | 3.17 | 6.85E-02 | 0.0026 | 4.55E-03 | 2.95E-13 | 100 | 56.7 | 1.80 | 0.00 | 22.8 ± 0.06 | 3.18E-01 | 8.71E-05 | 1.45E-03 | 4.66E-06 |

[a]Correction factors: $(^{40}Ar/^{39}Ar)_K = 0.025$, $(^{39}Ar/^{37}Ar)_{Ca} = 7 \times 10^{-4}$, $(^{36}Ar/^{37}Ar)_{Ca} = 2.5 \times 10^{-4}$.
[b]Corrected for backgrounds, mass discrimination, abundance sensitivity, and radioactive decay.
[c]Normalized to 100% delivery to mass spectrometer.
[d]Includes contribution from static line blank.
[e]Corrected for atmospheric argon and nucleogenic interferences.
[f]Assumes trapped argon is atmospheric.
[g]Corrected for nucleogenic interferences.
[h]Read 5.33E-01 as $5.33 \times 10^{-1}$.

22.6 ± 0.1 Ma (1σ) (Figure 9; Table 2). Volcanic rocks of similar age have been dated previously by the $^{40}Ar/^{39}Ar$ method near Shiquanhe (18–20 Ma) [*Arnaud and Vidal*, 1990] and 100 to 200 km to the east and southeast within the west central Lhasa terrane (18–23 Ma) [*Miller et al.*, 1999]. As the locality and uncertainty on the K-Ar whole rock age (~38 Ma) for the Zuozuo volcanic rocks are not provided [*Cheng and Xu*, 1987], it is not clear whether they are part of the volcanic unit mapped in this study (Tv).

## 5. Deformation History of the Shiquanhe Area

### 5.1. Assumptions

[33] The cross section of the Shiquanhe area (Figure 5) is based on stratigraphic thicknesses measured by *Cheng and Xu* [1987] or calculated from our bedding measurements, and its restoration is shown in Figure 10. The near-surface cross section (top 4 km) is reasonably constrained due to widespread preservation of Aptian-Albian limestones across the Shiquanhe thrust belt. The latter provide useful strain markers, from which minimum magnitudes of post-mid-Cretaceous shortening can be estimated. The shortening estimates are minimums for two reasons. First, the cross section does not incorporate mesoscale folds and faults or microstrain. Second, while the positions of footwall cutoffs can be inferred from stratigraphic thicknesses (such as the contact between the lower and upper parts of the Cretaceous unit), corresponding hanging wall cutoffs are lacking due to erosion. The restoration is based on the minimum slip necessary to restore rocks to horizontal.

[34] The cross section is poorly constrained at depth. Major assumptions were made in attempt to explore possible subsurface structure: (1) The cross section is assumed to be pinned at the south, where Cretaceous strata are shallow dipping and weakly deformed. While this assumption does not impact shortening estimates and is logical for addressing the south directed thrust system, it may be inappropriate for interpreting how the Narangjiapo thrust roots at depth. Consequently, the location of the Longzi La granite and the decollement between Permian and pre-Permian rocks in the footwall of the Narangjiapo thrust shown should be considered speculative. (2) Granitoids are common in the Shiquanhe area, and likely compose large portions of the deeper crust. For simplicity, however, only the Longzi La granite is shown in the cross section. Potential crustal thickening or strain localization related to emplacement of igneous bodies is not addressed. (3) Data are insufficient to distinguish between the two end-member models that Shiquanhe melange represents an in situ suture zone or materials obducted onto the Lhasa terrane from a suture zone to the north. The latter model is favored in the cross section, in that we assume the ophiolitic melange is a relatively thin lithotectonic unit of uniform thickness that structurally overlies Jurassic and older strata of the Lhasa terrane. As this assumption is unsubstantiated, the cross section is meant only to explore possible regional implications of our studies in the case that a thin-skinned fold and thrust belt model is applicable. Assumptions regarding crustal structure at depth, however, do not affect the minimum

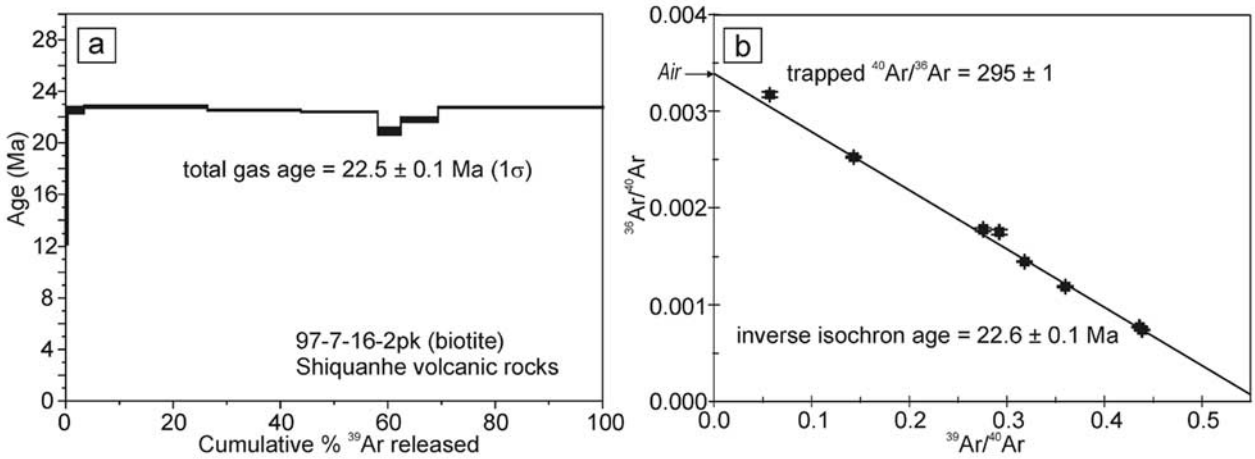


**Figure 9.** $^{40}Ar/^{39}Ar$ step-heating results for biotite separated from the Tertiary volcanic unit, Tv, at locality 7-16-2 shown in Foldout 1. (a) Age spectrum. (b) Inverse isochron plot. The total gas age is calculated by weighting the apparent ages for individual heating steps by the fraction of $^{39}Ar$ released. Regression of step-heating results on an inverse isochron diagram yields an inverse isochron age (X-intercept) and the composition of trapped $^{40}Ar/^{36}Ar$ (Y-intercept).

shortening estimates, as the latter are based on restoration of the widely exposed Cretaceous strata.

### 5.2. Kinematic History

[35] Palinspastic restoration of the Shiquanhe cross section suggests that ophiolitic melange and structurally overlying Jurassic flysch strata were obducted southward onto the northern margin of the Lhasa terrane prior to deposition of Lower Cretaceous strata (Figure 10a). If the ophiolitic melange represents an in situ suture zone rather than an obducted sheet (as assumed), the suture must have closed prior to being overlapped by Lower Cretaceous strata.

[36] The Narangjiapo thrust is interpreted to have placed the Longzi La granite and the Permian strata that it intrudes northward over ophiolitic melange and Cretaceous strata shortly before or during accelerated cooling of the Longzi La granite between 75 and 65 Ma (Figure 10b). The width of the exposed Narangjiapo thrust sheet and the magnitude of stratigraphic separation across it suggest >20 km of shortening. The Narangjiapo thrust may be related to a regional system of north directed thrusts in the central Lhasa terrane that juxtapose Paleozoic strata northward over Jurassic-Cretaceous rocks. These include the Shibaluo thrust near Coqin [*Murphy et al.*, 1997] and a south dipping thrust near Xainza that cuts ultramafic rocks in its footwall [*Girardeau et al.*, 1985] (Figure 2).

[37] The Zaduo thrust and the north dipping imbricate thrust system to the north involve only ophiolitic melange and Cretaceous strata in their hanging walls. This suggests a decollement at shallow structural levels near the unconformity between melange and Cretaceous strata (Figure 5). This decollement must ramp deeper to the north in order to juxtapose the Jurassic flysch strata over the Cretaceous strata along the Jaggang thrust. Cross-section restoration suggests that south directed, thin-skinned folding and thrusting accommodated >40 km of shortening (Figure 10c). Crosscutting relationships show that the south directed Zaduo thrust is younger than the Narangjiapo thrust but older than the Shiquanhe thrust (which cuts ~23 Ma volcanic rocks). Therefore, thin-skinned south directed thrusting occurred between 75 and 23 Ma, and perhaps mostly during the inferred episode of regional rapid cooling between 75 and 60 Ma.

[38] Cretaceous strata are at nearly the same structural level across the Shiquanhe thrust belt and in the less-deformed foreland south of the Shiquanhe thrust (Figure 5). This observation favors the interpretation that shortening below the thrust flats was accommodated by lateral translation as opposed to internal deformation of footwall rocks, because crustal thickening associated with internal shortening would be expected to elevate the structural level of Cretaceous strata in the thrust belt with respect to that in the foreland. Having the restoration be pinned on the south side emphasizes the possibility for significant underthrusting of Jurassic and older strata of the Lhasa terrane northward beneath allochthonous Jurassic flysch strata that structurally overlie the ophiolitic melange (Figure 10).

[39] The Shiquanhe thrust is the youngest fault mapped. The timing of slip along it is inferred from crosscutting relationships and basin analysis. The Shiquanhe thrust cuts ~23 Ma volcanic rocks in its footwall and therefore must have been active after Oligocene time. Paleocurrent indicators and compositions of clasts in Tertiary conglomerates that underlie the volcanic rocks are consistent with derivation from rocks in the hanging wall of the Shiquanhe thrust. Therefore, we suggest that slip along the Shiquanhe thrust was coeval with, and directly responsible for, basin development. This inference, together with the assumption of a continuous slip history for the Shiquanhe thrust, implies that the deformed fluvial strata in the footwall of the Shiquanhe thrust are Oligocene.

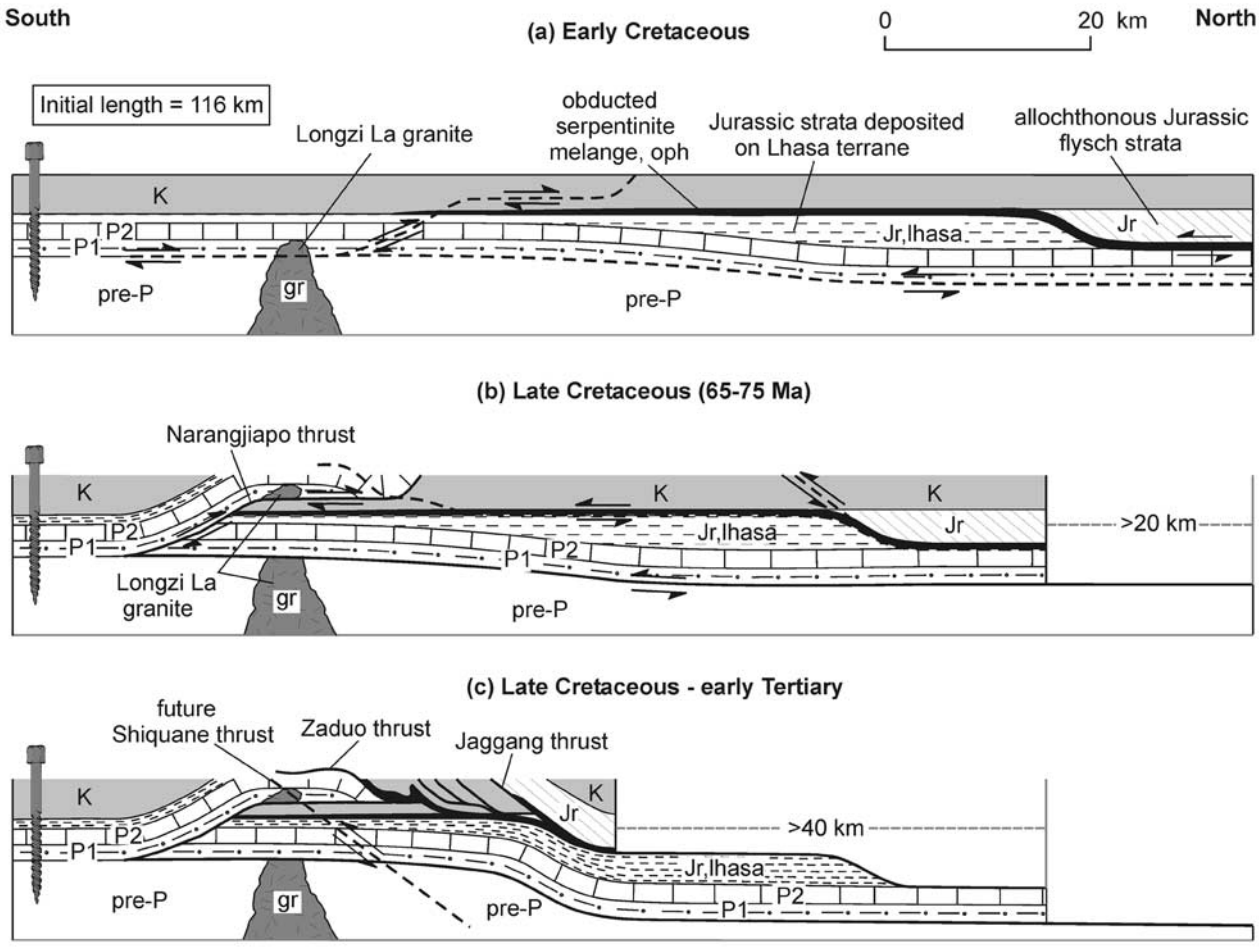


**Figure 10.** Palinspastic restoration of the Shiquanhe cross section (Figure 5). (a) Southward obduction of the melange sheet and structurally overlying Jurassic flysch strata onto the Lhasa terrane margin prior to deposition of Lower Cretaceous strata. (b) >20 km shortening along the north directed Narangjiapo thrust during Late Cretaceous time. (c) >40 km south directed thin-skinned thrusting along the Zaduo thrust and Jaggang thrust system during Late Cretaceous-early Tertiary time. Restoration is pinned on the south side to explore possible northward underthrusting of Jurassic and older rocks of the Lhasa terrane.

[40] The Shiquanhe thrust must root deep enough to bury the south dipping Narangjiapo thrust ramp and Tertiary basin fill, and therefore likely cuts the decollement for the south directed thrust belt at depth (Figure 5). A deeply rooted Shiquanhe thrust may explain the localized deposition of Tertiary strata. Minimum throw across the Shiquanhe thrust is constrained from the thickness of Tertiary basin fill in the footwall. The latter is estimated to be ~2.5 km structurally beneath the Shiquanhe thrust along the line of the cross section based on projection of bedding measurements to depth (Foldout 1). The thermal history calculated for the hanging wall Longzi La granite suggests that it cooled to below 150°C by ~65 Ma (Figure 8d). This result, together with the assumption of a 25°C/km geothermal gradient, suggests a maximum throw of 6 km across the Shiquanhe fault in excess of that required to bury the Tertiary strata. Under the assumption of a planar fault that dips 40°, the above limits on throw suggest that the Shiquanhe thrust accommodated between 3 and 10 km of Cenozoic shortening (~7 km of shortening is shown in the cross section; Figure 5).

## 6. Regional Cross Section

[41] The cross section of the Bangong-Nujiang suture zone in western Tibet (Figure 12) is an extension of the Shiquanhe area cross section (A-A″, Figure 5) northward to the southern Qiangtang terrane (A‴, see Figure 11 for location). The cross section is highly speculative, as it is based on our interpretations of reconnaissance-style mapping [*Cheng and Xu*, 1987; *Liu*, 1988; *Matte et al.*, 1996] and the same assumptions that were used to construct the Shiquanhe cross section (see section 5.1.). Perhaps the least substantiated assumption is that exposures of ophiolitic melanges in western Tibet were part of a once continuous and relatively thin sheet. However, we show that the restored regional cross section (Figure 13a) implies a rather simple tectonic configuration for the Bangong-Nujiang

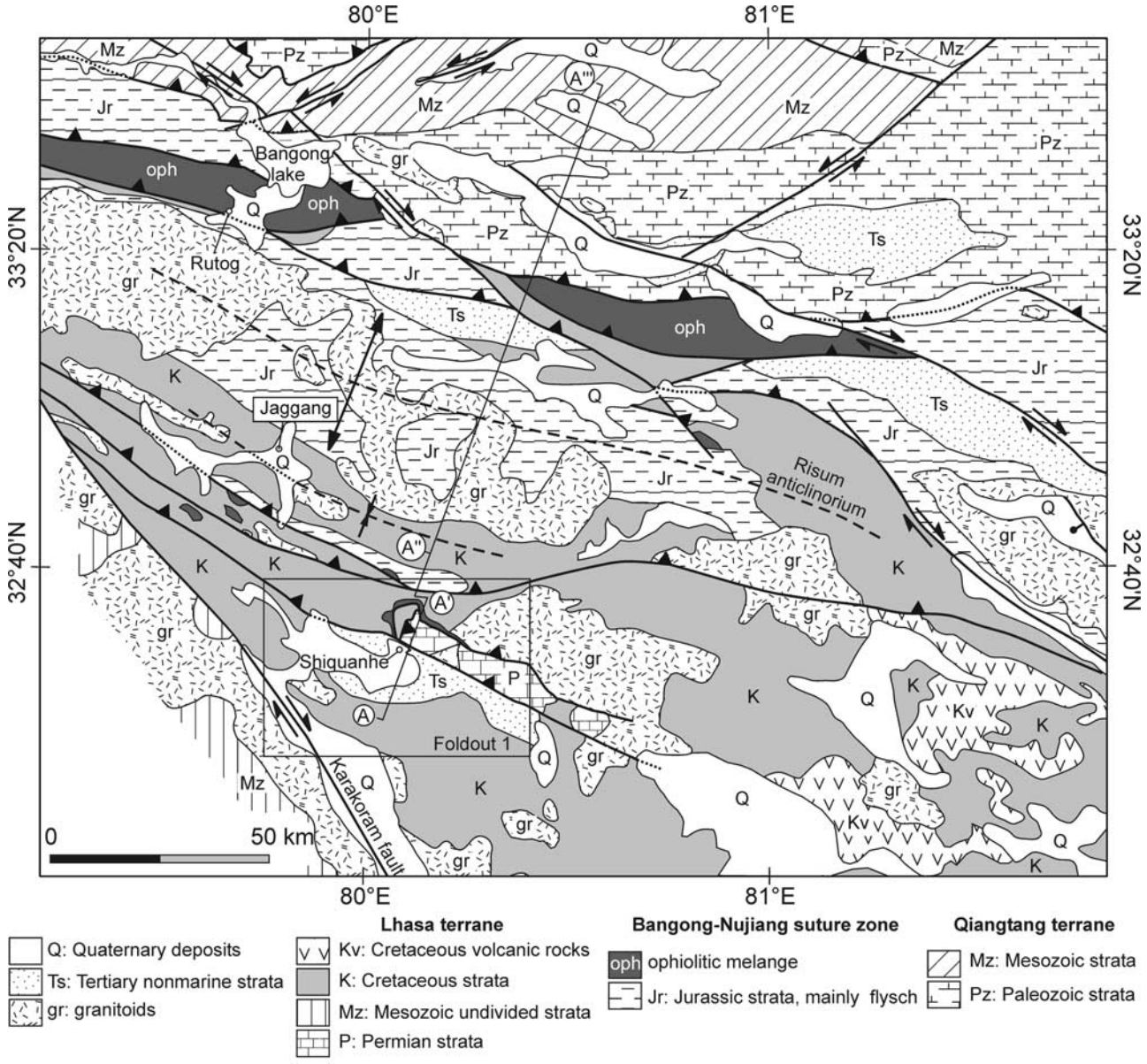


**Figure 11.** Geologic map of the Shiquanhe-Rutog region compiled from *Cheng and Xu* [1987] and *Liu* [1988], with our structural interpretations added.

suture zone prior to Late Cretaceous thrusting (Figure 14) that is compatible with the regional geology. In addition, the restoration provides useful first-order minimum estimates of shortening that are independent of assumptions regarding the distribution of ophiolitic melange at depth.

[42] Shortening in the Shiquanhe area may be directly linked with formation of the Risum anticlinorium. Our studies suggest that thrusts in the Shiquanhe area accommodated >67 km of upper crustal north south shortening (57% shortening over the 50-km-long cross section shown in Figure 5) during Late Cretaceous-early Tertiary time. In contrast, Late Cretaceous-early Tertiary deformation to the north is characterized by formation of the ~50-km-wide, Jurassic-flysch-cored Risum anticlinorium. Lhasa terrane rocks below the thrust flats in the Shiquanhe area are proposed to have accommodated shortening by underthrusting northward beneath the allochthonous Jurassic flysch (Figure 10c). The minimum magnitude of inferred underthrusting of Permian and Jurassic strata (40 km) is equal to the minimum magnitude of shortening needed to form the ~50-km-wide Risum anticlinorium by duplexing of underthrust Lhasa terrane Permian strata (Figure 12). The weak, subhorizontal sheet of ophiolitic melange may have served (1) to transfer crustal shortening in the Shiquanhe area northward relative to the Jurassic flysch strata and to deeper structural levels and, (2) as a roof thrust to the duplex that formed the Risum anticlinorium. Alternatively, the Risum anticlinorium may have formed by penetrative deformation of Jurassic flysch above a thrust flat which fed slip southward to thrusts in the Shiquanhe area. This model would provide a

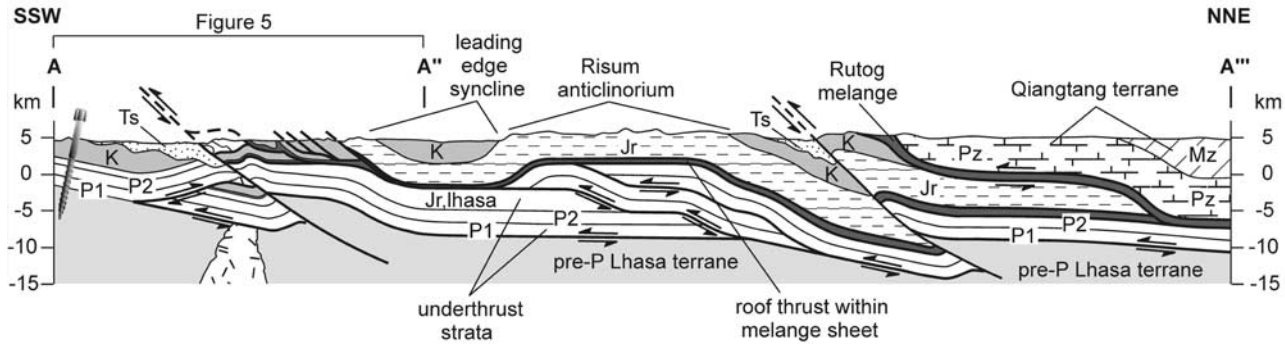


**Figure 12.** Regional north-south cross section of the Bangong-Nujiang suture zone in western Tibet. See Figure 11 for line of section and the text for major assumptions that were made to construct the cross section.

minimum estimate for shortening that is greater by ~20 km (based on area balancing) than what is shown in Figure 13.

[43] The most significant tectonic boundary north of the Risum anticlinorium is a north dipping thrust that places Paleozoic and Mesozoic strata of the Qiangtang terrane in the hanging wall against ophiolitic melange and Jurassic flysch of the Rutog melange zone in the footwall. The magnitude of shortening across this fault is difficult to constrain because shallow marine Cretaceous strata are absent in the Qiangtang terrane to the north [*Liu*, 1988] (Figure 11). We tentatively propose an estimate of 35 km (Figure 12), based on down-plunge projection of footwall Jurassic flysch strata exposed east of the Rutog melange into the line of section (Figure 11). A portion of this shortening could have been balanced by deformation of Cretaceous strata immediately south of the Rutog melange zone (Figure 12), which has been described by previous workers [*Ratschbacher et al.*, 1994; *Matte et al.*, 1996] but is not represented on regional geologic maps.

[44] Restoration of the regional cross section suggests that the melange sheet and overlying allochthonous Jurassic flysch strata may have been obducted >185 km southward onto the northern margin of the Lhasa terrane prior to deposition of Lower Cretaceous strata (Figure 13a). Following obduction, deformation stepped to the north near Rutog. Here, a thrust system is interpreted to have (1) imbricated the melange sheet, and (2) accommodated an unconstrained amount of southward underthrusting of the Lhasa terrane beneath the Qiangtang terrane. During Late Cretaceous-earliest Tertiary time, thrusts in the Shiquanhe area, formation of the Risum anticlinorium, and deformation within the Rutog melange zone are suggested to have accommodated >77 km of shortening (Figure 13c). It is possible that a significant portion of this shortening was accommodated in the deeper crust by additional northward underthrusting of the Lhasa terrane beneath the Qiangtang terrane.

## 7. Discussion

### 7.1. Significance of the Shiquanhe Thrust

[45] The Shiquanhe fault has been proposed to be part of a dextral wrench zone that transfers slip from the Miocene to Recent Karakoram fault to north trending rifts in southwestern Tibet [*Ratschbacher et al.*, 1994], a Neogene to Quaternary thrust [*Cheng and Xu*, 1987; *Matte et al.*, 1996], and a Miocene thrust linked with the right-slip Karakoram fault [*Murphy et al.*, 2000]. Our studies demonstrate that the Shiquanhe fault is a south directed thrust and cuts flat-lying ~23 Ma volcanic rocks and underlying deformed Tertiary fluvial strata in its footwall. Deposition and deformation of the Tertiary basin fill occurred during at least Oligocene time, if our assumption of a continuous slip history for the Shiquanhe thrust is correct. This interpretation suggests that the Shiquanhe thrust was contemporaneous with the Gangdese thrust system of southern Tibet [*Yin et al.*, 1994, 1999a; *Harrison et al.*, 2000], and implies coeval modification of the Bangong-Nujiang and Indus-Yalu suture zones by south directed thrusting during the Oligocene. While the youngest slip on the Shiquanhe thrust occurred after 23 Ma, thermochronologic results on the Longzi La granite limit Neogene throw to ~6 km. Therefore, if the Shiquanhe thrust transferred slip from the Karakoram fault system during Miocene time [*Murphy et al.*, 2000], it can explain only a small fraction of the >80 km of north south shortening needed in western Tibet to resolve differences in slip estimates for the central [*Searle et al.*, 1998] and southern [*Murphy et al.*, 2000] Karakoram fault. Perhaps this shortening was accommodated

**Figure 13.** (opposite) Palinspastic restoration of the regional cross section shown in Figure 12. Black, gray, and dashed faults are active, inactive, and future faults, respectively. (a) The ophiolitic melange sheet and overlying Jurassic flysch strata were obducted ~185 km onto the Lhasa terrane margin prior to deposition of Lower Cretaceous strata. (b) North directed thrusting along the Narangjiapo thrust during Late Cretaceous time. (c) Late Cretaceous-early Tertiary south directed thrusting and formation of the Risum anticlinorium by duplexing of underthrust Permian strata of the Lhasa terrane beneath it. (d) South directed thrusting and development of nonmarine basins during Oligocene-Miocene time. Restoration is pinned on the south side to illustrate possible underthrusting of the Lhasa terrane northward beneath the Qiangtang terrane.

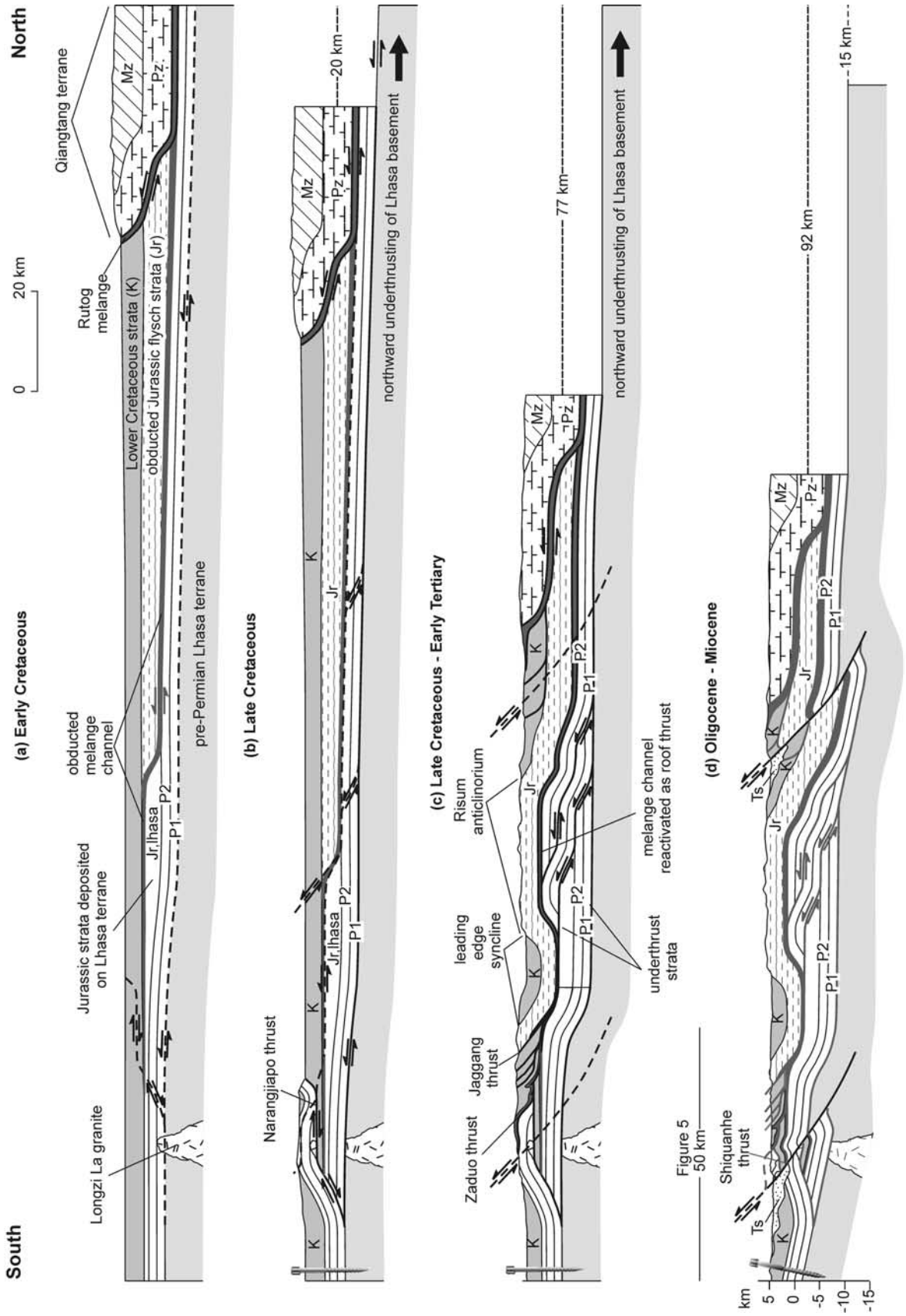
South
North
(a) Early Cretaceous
0
20 km
Qiangtang terrane
Rutog melange
Mz
Pz
Lower Cretaceous strata (K)
obducted Jurassic flysch strata (Jr)
obducted melange channel
Jurassic strata deposited on Lhasa terrane
Jr,lhasa
P2
P1
pre-Permian Lhasa terrane
Longzi La granite
(b) Late Cretaceous
20 km
Mz
Pz
K
Jr
northward underthrusting of Lhasa basement
Narangjiapo thrust
Jr,lhasa
P2
P1
(c) Late Cretaceous - Early Tertiary
77 km
Mz
Pz
K
Jr
P2
P1
northward underthrusting of Lhasa basement
Risum anticlinorium
leading edge syncline
melange channel reactivated as roof thrust
underthrust strata
Zaduo thrust
Jaggang thrust
(d) Oligocene - Miocene
92 km
15 km
Mz
Pz
K
Jr
P2
P1
Ts
Shiquanhe thrust
Figure 5
50 km
km
5
0
-5
-10
-15

by thrusts, which have not yet been recognized, within the Risum anticlinorium and Rutog melange belt to the north.

### 7.2. Tectonic Evolution of the Bangong-Nujiang Suture Zone in Western Tibet

[46] An in situ suture zone model for the tectonic significance of Shiquanhe ophiolitic melange remains viable and warrants consideration in future studies. However, the regional geology of western Tibet may be explained more simply in terms of a single, north dipping convergent margin system that was obducted southward onto the margin of the Lhasa terrane during Late Jurassic-Early Cretaceous time and shortened significantly during Late Cretaceous-early Tertiary collision between the Lhasa and Qiangtang terranes. In the following, we present in more detail this model and its regional implications.

[47] The inferred sheet of ophiolitic melange and structurally overlying Jurassic flysch strata in western Tibet represent remnants of a north dipping subduction-accretion complex and structurally overlying forearc basin fill that were deposited mainly on ophiolitic basement (Figure 14a). The melange sheet and overlying forearc were obducted southward onto Jurassic and Permian strata of the northern margin of the Lhasa terrane during Late Jurassic-Early Cretaceous closure of the Bangong-Nujiang Ocean (Figure 14b). The ophiolitic fragments in the melange were sourced from the forearc oceanic basement by tectonic erosion during both oceanic subduction (Figure 14a) and subsequent obduction. Thrusting stepped to the north of the obducted sheet during Early Cretaceous time, marking the initiation of continental collision between the Lhasa and Qiangtang terranes, and repeated the ophiolitic melange sheet in the Rutog area (Figure 14c). The Lower Cretaceous strata that lie unconformable on older Lhasa terrane rocks and the obducted melange and forearc were deposited in a flexural foreland basin related to Lhasa-Qiangtang collision, as previously suggested [*Leeder et al.*, 1988; *Yin et al.*, 1994]. The obducted melange sheet served as a decollement to thrusts in the Shiquanhe area and as a roof thrust or basal detachment below Jurassic flysch of the Risum anticlinorium during Late Cretaceous-earliest Tertiary intracontinental deformation. Cretaceous magmatism near Shiquanhe and to the north is related to northward oceanic subduction along the Indus-Yalu suture to the south. Blocks of Aptian limestones may have been tectonically incorporated into ophiolitic melanges near Rutog [*Matte et al.*, 1996] during intracontinental deformation, and therefore may not provide a maximum age for final closure of the Bangong-Nujiang Ocean.

[48] Our model for the origin of Shiquanhe ophiolitic melange differs from the nappe hypothesis proposed for the Dongqiao and Xainxa ophiolitic rocks north of Lhasa [*Girardeau et al.*, 1984; *Girardeau et al.*, 1985; *Coward et al.*, 1988] in two ways. First, the ophiolitic materials do not represent fragments of a single sheet of obducted oceanic lithosphere, but rather tectonic blocks within a melange. Second, our model predicts that during obduction, ophiolitic melange was structurally beneath as opposed to structurally above Jurassic flysch strata. Ophiolitic melange can be thrust over Jurassic flysch, but in these cases the thrusts should postdate obduction. These predictions are consistent with the regional geologic map of western Tibet, which shows that (1) ophiolitic materials do not occur on the limbs of the Risum anticlinorium, along the unconformable contacts between Jurassic and Cretaceous strata, and (2) thrusts that place ophiolitic melange over Jurassic flysch involve post-obduction Albian-Aptian strata [*Liu*, 1988] (Figure 11).

### 7.3. Formation of the Qiangtang Anticlinorium

[49] The regional map pattern of the Qiangtang terrane can be explained by the east plunging Qiangtang anticlinorium, which is characterized by metamorphic rocks and Paleozoic strata in its core and Mesozoic strata along its limbs (Figure 2) [*Kapp et al.*, 2000; *Yin and Harrison*, 2000]. Just as northward underthrusting of Jurassic and older strata of the Lhasa terrane could have produced the Risum anticlinorium (Figure 13), the Qiangtang anticlinorium may have formed because of northward continental underthrusting of the Lhasa terrane beneath the Qiangtang terrane [*Yin and Harrison*, 2000] (Figures 14c and 14d). Continental underthrusting may have been facilitated by slip within the obducted melange sheet. The systematic correspondence between westward narrowing of the Lhasa terrane with westward widening of the Qiangtang anticlinorium may imply an increase in the magnitude of continental underthrusting of the Lhasa terrane beneath the Qiangtang terrane toward the west [*Yin and Harrison*, 2000]. This raises the intriguing possibility that the apparent absence of Permian and older rocks of the continental Lhasa terrane in the Karakoram range may be a result of it having been completely underthrust beneath the Karakoram terrane to the north. Ongoing studies are suggesting that growth of the Qiangtang anticlinorium initiated prior to widely dis-

**Figure 14.** (opposite) Model for the Late Jurassic-early Tertiary tectonic evolution of the Bangong-Nujiang suture zone in western Tibet. Note that the boxes outline illustrations that are at different scales. (a) Ophiolitic melange and allochthonous Jurassic flysch strata in western Tibet represent a subduction-accretion complex and forearc basin fill, respectively, that developed above a single north dipping oceanic subduction zone along the southern margin of the Qiangtang terrane. Ophiolitic fragments are tectonically eroded from the oceanic basement to the forearc basin and incorporated into the melange. (b) Late Jurassic-Early Cretaceous closure of the Bangong-Nujiang Ocean and obduction of the melange sheet and forearc basin fill onto the northern margin of the Lhasa terrane. (c) During Early Cretaceous time, thrusting stepped to the north of the obducted sheet. It accommodated northward underthrusting of the Lhasa terrane beneath the Qiangtang terrane and was linked with development of the Qiangtang anticlinorium. Lower Cretaceous strata were deposited in a flexural foreland basin. (d) Continued northward underthrusting of the Lhasa terrane beneath the Qiangtang terrane and further growth of the Qiangtang anticlinorium during Late Cretaceous-early Tertiary time. Note that imbrication of the obducted ophiolitic melange sheet produces two belts separated by ~100 km in western Tibet.

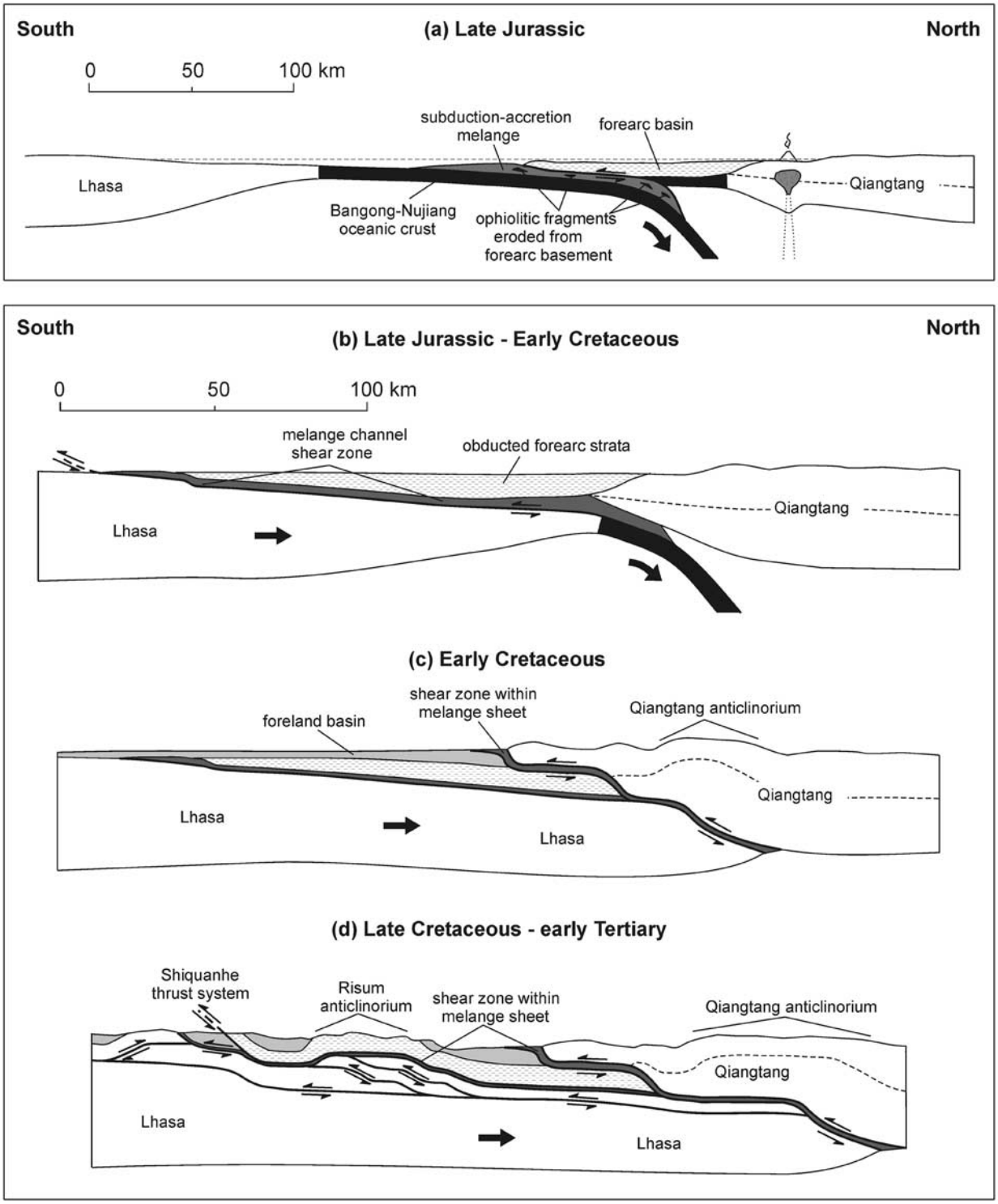
South
(a) Late Jurassic
North
0
50
100 km
subduction-accretion melange
forearc basin
Lhasa
Qiangtang
Bangong-Nujiang oceanic crust
ophiolitic fragments eroded from forearc basement
South
(b) Late Jurassic - Early Cretaceous
North
0
50
100 km
melange channel shear zone
obducted forearc strata
Lhasa
Qiangtang
(c) Early Cretaceous
shear zone within melange sheet
foreland basin
Qiangtang anticlinorium
Qiangtang
Lhasa
Lhasa
(d) Late Cretaceous - early Tertiary
Shiquanhe thrust system
Risum anticlinorium
shear zone within melange sheet
Qiangtang anticlinorium
Qiangtang
Lhasa
Lhasa

tributed 120 to 105 Ma volcanism and continued until at least Oligocene time [*Kapp et al.*, 2002].

### 7.4. Implications for Crustal Thickening

[50] Widely exposed Albian-Aptian shallow marine strata suggest that the Bangong-Nujiang suture zone was near sea level during mid-Cretaceous time, and was likely underlain by ~35-km thick crust. Restoration of the 160-km-wide regional cross-section of western Tibet suggests >92 km of post-mid-Cretaceous shortening, a substantial portion of which likely occurred prior to or during the earliest stages of the Indo-Asian collision (>37% shortening; Figures 12 and 13). Under the assumption of homogeneous crustal thickening, this shortening would have produced >20 km of crustal thickening, minus denudation. The latter is likely <6 km based on thermochronologic studies [*Matte et al.*, 1996; this study] and the low-grade metamorphism exhibited by exposed rocks. Given that our shortening estimate is a minimum, it is possible that homogeneous crustal thickening was the dominant crustal thickening mechanism of the western Bangong-Nujiang suture zone. An end-member alternative, suggested in our tectonic reconstruction (Figure 14), is that Late Cretaceous-early Tertiary upper crustal shortening across the Bangong-Nujiang suture zone was accommodated in the deeper crust by northward underthrusting. This model provides a mechanism to significantly thicken the central Tibetan crust, without violating observations of minor upper crustal shortening within the western Qiangtang terrane [*Matte et al.*, 1996], and implies that the deeper southern Tibetan crust was thickened significantly by Tertiary underthrusting or injection of Indian crust [*Zhao and Morgan*, 1987; *Owens and Zandt*, 1997; *DeCelles et al.*, 2002].

## 8. Conclusions

[51] Restoration of deformation that involves widely distributed mid-Cretaceous strata in southern Tibet has unique potential to provide minimum estimates of post-mid-Cretaceous shortening and to elucidate the tectonic configuration of southern Tibet during Early Cretaceous time. This is illustrated for far-western Tibet, where Cretaceous strata lie depositional on Jurassic flysch to the north, ophiolitic melange near Shiquanhe, and on older rocks of the Lhasa terrane to the south. Near Shiquanhe, field mapping and geochronologic studies document major Late Cretaceous-Tertiary north south shortening. Permian strata near Shiquanhe are intruded by the Longzi La granite, which yielded U-Pb ion-microprobe zircon ages between 161 and 124 Ma and experienced an episode of rapid cooling between 75 and 65 Ma. The Late Cretaceous Narangjiapo thrust is interpreted to have placed Permian strata and the Longzi La granite >20 km northward over ophiolitic melange and Lower Cretaceous strata. To the north, the south directed Jaggang thrust system roots into a decollement within ophiolitic melange and shortened Lower Cretaceous strata by >40 km. To the south, the Narangjiapo thrust is cut by the north dipping Shiquanhe thrust. In the footwall of the Shiquanhe thrust are folded Tertiary nonmarine strata and overlying, undeformed Oligo-Miocene (22.6 ± 0.3 Ma) volcanic rocks. The Shiquanhe thrust is estimated to have accommodated between 3 and 10 km of Cenozoic shortening, and was likely coeval with the Oligocene Gangdese thrust system of southern Tibet.

[52] Late Cretaceous-early Tertiary shortening in the Shiquanhe area may have been accommodated in the deeper crust by northward underthrusting and duplexing of Lhasa terrane rocks, which can help explain formation of the (1) ~50-km-wide, east-west trending Risum anticlinorium of Jurassic flysch ~60 km north of Shiquanhe, and (2) ~150-km-wide east plunging anticlinorium within the Qiangtang terrane, when additional Cretaceous-early Tertiary shortening along the Bangong-Nujiang suture zone to the north is included. We propose that continental underthrusting was facilitated by slip along a weak, subhorizontal sheet of ophiolitic melange that was obducted onto the Lhasa terrane during Late Jurassic-Early Cretaceous closure of the Bangong-Nujiang Ocean. The east-west belts of ophiolitic melanges exposed near Shiquanhe and ~100 km to the north may represent imbricates of this melange sheet as opposed to two distinct Mesozoic suture zones or remnants of a large ophiolite nappe.

[53] **Acknowledgments.** This research was supported by a U.S. NSF grant (EAR-98-05340, A. Yin and T. M. Harrison), a Chinese National Tibetan grant (1998040800, L. Ding), and a Geological Society of America student grant (P. Kapp). We thank Eric Cowgill and Oscar Lovera for assistance with the $^{40}Ar/^{39}Ar$ thermochronology and Brian Horton and Michael Taylor for their useful comments on this manuscript prior to submission. Reviews by David Evans, Kip Hodges, Terry Pavlis, and Brian Wernicke significantly improved this manuscript.

## References

Allègre, C. J., et al., Structure and evolution of the Himalaya-Tibet orogenic belt, *Nature*, *307*, 17–22, 1984.

Argand, E., La tectonique de L'Asie, *Proc. Int. Geol. Congr., XIII*, *7*, 171–372, 1924.

Armijo, R., P. Tapponnier, J. L. Mercier, and T.-L. Han, Quaternary extension in southern Tibet: Field observations and tectonic implications, *J. Geophys. Res.*, *91*, 13,803–13,872, 1986.

Armijo, R., P. Tapponnier, and H. Tonglin, Late Cenozoic right-lateral strike-slip faulting in southern Tibet, *J. Geophys. Res.*, *94*, 2787–2838, 1989.

Arnaud, N., and P. Vidal, Geochronology and geochemistry of the magmatic rocks from the Kunlun-Karakorum geotraverse, in *Colloque Kunlun-Karakorum, IPG, 52*, Inst. de Phys. du Globe, Paris, 1990.

Avouac, J.-P., and P. Tapponnier, Kinematic model of active deformation in central Asia, *Geophys. Res. Lett.*, *20*, 895–898, 1993.

Bird, P., Lateral extrusion of lower crust from under high topography, in the isostatic limit, *J. Geophys. Res.*, *96*, 10,275–10,286, 1991.

Burg, J. P., and G. M. Chen, Tectonics and structural zonation of southern Tibet, China, *Nature*, *311*, 219–223, 1984.

Burg, J.-P., F. Proust, P. Tapponnier, and G. M. Chen, Deformation phases and tectonic evolution of the Lhasa block (Southern Tibet, China), *Eclogae Geol. Helv.*, *76*, 643–665, 1983.

Burtman, V. S., and P. Molnar, Geological and geophysical evidence for deep subduction of continental crust beneath the Pamir, *Spec. Pap. Geol. Soc. Am.*, *281*, 76 pp., 1993.

Chang, C.-F., and S.-L. Zheng, Tectonic features of the Mount Jolmu Lungma region in southern Tibet, China (in Chinese), *Sci. Geol. Sinica*, *1*, 1–12, 1973.

Cheng, J., and G. Xu, Geologic map of the Gaize region with report, 369 pp., Tibetan Bur. of Geol. and Miner. Resour., Lhasa, 1986.

Cheng, J., and G. Xu, Geologic Map of the Ritu Region with report, 598 pp., Tibetan Bur. of Geol. and Miner. Resour., Lhasa, 1987.

Cherniak, D. J., and E. B. Watson, Pb diffusion in zircon, *Chem. Geol.*, *172*, 5–24, 2000.

Clark, M. K., and L. H. Royden, Topographic ooze: Building the eastern margin of Tibet by lower crustal flow, *Geology*, *28*, 703–706, 2000.

Compston, W., I. S. Williams, and C. Meyer, U-Pb Geochronology of zircons from Lunar Breccia 73217 using a sensitive high mass-resolution ion microprobe, *J. Geophys. Res.*, *89*, 525–534, 1984.

Coulon, C., H. Maluski, C. Bollinger, and S. Wang, Mesozoic and Cenozoic volcanic rocks from central and southern Tibet: $^{39}$Ar-$^{40}$Ar dating, petrological characteristics and geodynamical significance, *Earth Planet. Sci. Lett.*, *79*, 281–302, 1986.

Coward, M. P., and R. W. H. Butler, Thrust tectonics and the deep structure of the Pakistan Himalaya, *Geology*, *13*, 417–420, 1985.

Coward, M. P., W. S. F. Kidd, Y. Pan, R. M. Shackleton, and H. Zhang, The structure of the 1985 Tibet Geotraverse, Lhasa to Golmud, *Philos. Trans. R. Soc. London, Ser. A*, *327*, 307–336, 1988.

DeCelles, P. G., G. E. Gehrels, J. Quade, T. P. Ojha, P. A. Kapp, and B. N. Upreti, Neogene foreland basin deposits, erosional unroofing, and the kinematic history of the Himalayan fold-thrust belt, western Nepal, *Geol. Soc. Am. Bull.*, *110*, 2–21, 1998.

DeCelles, P. G., D. M. Robinson, J. Quade, T. P. Ojha, C. N. Garzione, P. Copeland, and B. N. Upreti, Stratigraphy, structure, and tectonic evolution of the Himalayan fold-thrust belt in western Nepal, *Tectonics*, *20*, 487–509, 2001.

DeCelles, P. G., D. M. Robinson, and G. Zandt, Implications of shortening in the Himalayan fold-thrust belt for uplift of the Tibetan Plateau, *Tectonics*, *21*(6), 1062, doi:10.1029/2001TC001322, 2002.

Dewey, J. F., and J. M. Bird, Mountain belts and the new global tectonics, *J. Geophys. Res.*, *75*, 2625–2647, 1970.

Dewey, J. F., and K. C. A. Burke, Tibetan, Variscan and Precambrian basement reactivation: Products of continental collision, *J. Geol.*, *81*, 683–692, 1973.

Dewey, J. F., R. M. Shackleton, C. Chengfa, and S. Yiyin, The tectonic evolution of the Tibetan Plateau, *Philos. Trans. R. Soc. London, Ser. A*, *327*, 379–413, 1988.

Dunlap, W. J., and R. Wysoczanski, Thermal evidence for early Cretaceous metamorphism in the Shyok suture zone and age of the Khardung volcanic rocks, Ladakh, India, *J. Asian Earth Sci.*, *20*, 481–490, 2002.

Dunlap, W. J., R. F. Weinberg, and M. P. Searle, Karakoram fault zone rocks cool in two phases, *J. Geol. Soc. London*, *155*, 903–912, 1998.

England, P., and G. Houseman, Finite strain calculations of continental deformation: 2, Comparison with the Indo-Asian collision zone, *J. Geophys. Res.*, *91*, 3664–3676, 1986.

Fielding, E., B. Isacks, M. Barazangi, and C. Duncan, How Flat is Tibet?, *Geology*, *22*, 163–167, 1994.

Girardeau, J., J. Marcoux, C. J. Allègre, J. P. Bassoullet, T. Youking, X. Xuchang, Z. Yougong, and W. Xibin, Tectonic environment and geodynamic significance of the Neo-Cimmerian Donqiao ophiolite, Bangong-Nujiang suture zone, Tibet, *Nature*, *307*, 27–31, 1984.

Girardeau, J., J. Marcoux, E. Fourcade, J. P. Bassoullet, and T. Youking, Xainxa ultramafic rocks, central Tibet, China: Tectonic environment and geodynamic significance, *Geology*, *13*, 330–333, 1985.

Harris, N. B. W., X. Ronghua, C. L. Lewis, C. J. Hawkesworth, and Z. Yuquan, Isotope geochemistry of the 1985 Tibet Geotraverse, Lhasa to Golmud, *Philos. Trans. R. Soc. London, Ser. A*, *327*, 263–285, 1988.

Harris, N. B. W., S. Inger, and X. Ronghua, Cretaceous plutonism in Central Tibet: An example of post-collision magmatism?, *J. Volcanol. Geotherm. Res.*, *44*, 21–32, 1990.

Harrison, T. M., M. T. Heizler, O. M. Lovera, W. Chen, and M. Grove, A chlorine disinfectant for excess argon released from K-feldspar during step heating, *Earth Planet. Sci. Lett.*, *123*, 95–104, 1994.

Harrison, T. M., A. Yin, M. Grove, O. M. Lovera, F. J. Ryerson, and X. Zhou, The Zedong Window: A record of superposed Tertiary convergence in southeastern Tibet, *J. Geophys. Res.*, *105*, 19,211–19,230, 2000.

Hodges, K. V., Tectonics of the Himalaya and southern Tibet from two perspectives, *Geol. Soc. Am. Bull.*, *112*, 324–350, 2000.

Hsü, K. J., P. Guitang, and A. M. C. Sengör, Tectonic Evolution of the Tibetan Plateau: A working hypothesis based on the Archipelago model of orogenesis, *Int. Geol. Rev.*, *37*, 473–508, 1995.

Kapp, P., M. Murphy, A. Yin, and D. Lin, Cenozoic shortening along the Banggong-Nujiang suture zone, central Tibet, paper presented at 14th Himalaya-Karakorum-Tibet Workshop, Univ. of Tubingen, Kloster Ettal, Germany, 1999.

Kapp, P., A. Yin, C. E. Manning, M. Murphy, T. M. Harrison, M. Spurlin, L. Ding, X.-G. Deng, and C.-M. Wu, Blueschist-bearing metamorphic core complexes in the Qiangtang block reveal deep crustal structure of northern Tibet, *Geology*, *28*, 19–22, 2000.

Kapp, P., A. Yin, T. M. Harrison, and L. Ding, Cretaceous-Tertiary deformation history of central Tibet, *Geol. Soc. Am. Abstr. Programs*, *34*, 487, 2002.

Kidd, W. S. F., and P. Molnar, Quaternary and active faulting observed on the 1985 Academia Sinica-Royal Society Geotraverse of Tibet, *Philos. Trans. R. Soc. London, Ser. A*, *327*, 337–363, 1988.

Kidd, W. S. F., Y. Pan, C. Chang, M. P. Coward, J. F. Dewey, F. R. S., A. Gansser, P. Molnar, R. M. Shackleton, and Y. Sun, Geological mapping of the 1985 Chinese-British Tibetan (Xizang-Qinghai) Plateau Geotraverse route, *Philos. Trans. R. Soc. London, Ser. A*, *327*, 287–305, 1988.

Kirby, E., K. X. Whipple, B. C. Burchfiel, W. Tang, G. Berger, Z. Sun, and Z. Chen, Neotectonics of the Min Shan, China: Implications for mechanisms driving Quaternary deformation along the eastern margin of the Tibetan Plateau, *Geol. Soc. Am. Bull.*, *112*, 375–393, 2000.

Leeder, M. R., A. B. Smith, and Y. Jixiang, Sedimentology and palaeoenvironmental evolution of the 1985 Lhasa to Golmud geotraverse, *Philos. Trans. R. Soc. London, Ser. A*, *327*, 107–143, 1988.

Liu, Z. Q. C., Geologic Map of the Qinghai-Xizang Plateau and its Neighboring Regions (scale at 1:1,500,000), Geol. Publ. House, Beijing, 1988.

Lovera, O. M., F. M. Richter, and T. M. Harrison, The $^{40}$Ar/$^{39}$Ar thermochronometry for slowly cooled samples having a distribution of diffusion domain sizes, *J. Geophys. Res.*, *94*, 17,917–17,935, 1989.

Lovera, O. M., M. Grove, T. M. Harrison, and K. I. Mahon, Systematic analysis of K-feldspar $^{40}$Ar/$^{39}$Ar step-heating experiments: I. Significance of activation energy determinations, *Geochim.Cosmochim. Acta*, *61*, 3171–3192, 1997.

Lovera, O. M., M. Grove, and T. M. Harrison, Systematic analysis of K-feldspar $^{40}$Ar/$^{39}$Ar step heating results: II. Relevance of laboratory argon diffusion properties to nature, *Geochim. Cosmochim. Acta*, *66*, 1237–1255, 2002.

Matte, P., P. Tapponnier, N. Arnaud, L. Bourjot, J. P. Avouac, P. Vidal, Q. Liu, Y. Pan, and Y. Wang, Tectonics of Western Tibet, between the Tarim and the Indus, *Earth Planet. Sci. Lett.*, *142*, 311–330, 1996.

Mei, H. J., X. N. Lin, J. X. Chi, G. Y. Zhang, and M. T. Wu, On ophiolite system on Qinghai-Xizang plateau with particular reference to its genesis in West Xizang, *Geol. Ecol. Stud. Xinghai-Xizang Plateau, Proc. Symp. Qinghai-Xizang (Tibet) Plateau*, *1*, 545–556, 1981.

Métivier, F., Y. Gaudemer, P. Tapponnier, and B. Meyer, Northeastward growth of the Tibet plateau deduced from balanced reconstruction of two depositional areas: The Qiadam and Hexi Corridor basins, China, *Tectonics*, *17*, 823–842, 1998.

Meyer, B., P. Tapponnier, L. Bourjot, F. Métivier, Y. Gaudemer, G. Peltzer, S. Guo, and Z. Chen, Crustal thickening in Gansu-Qinghai, lithospheric mantle subduction, and oblique, strike-slip controlled growth of the Tibet plateau, *Geophys. J. Int.*, *135*, 1–47, 1998.

Miller, C., R. Schuster, U. Klotzli, W. Frank, and F. Purtscheller, Post-collisional potassic and ultrapotassic magmatism in SW Tibet: Geochemical and Sr-Nd-Pb-O isotopic constraints for mantle source characteristics and petrogenesis, *J. Petrol.*, *40*, 1399–1424, 1999.

Murphy, M. A., A. Yin, T. M. Harrison, S. B. Dürr, Z. Chen, F. J. Ryerson, W. S. F. Kidd, X. Wang, and X. Zhou, Did the Indo-Asian collision alone create the Tibetan plateau?, *Geology*, *25*, 719–722, 1997.

Murphy, M. A., A. Yin, P. Kapp, T. M. Harrison, D. Lin, and G. Jinghui, Southward propagation of the Karakoram fault system, southwest Tibet: Timing and magnitude of slip, *Geology*, *28*, 451–454, 2000.

Owens, T. J., and G. Zandt, Implications of crustal property variations for models of Tibetan plateau evolution, *Nature*, *387*, 37–43, 1997.

Paces, J. B., and J. D. Miller, Precise U-Pb age of Duluth Complex and related mafic intrusions, northeastern Minnesota: Geochronological insights into physical, petrogenetic, paleomagnetic, and tectonomagmatic processes associated with the 1.1 Ga midcontinent rift system, *J. Geophys. Res.*, *98*, 13,997–14,013, 1993.

Pan, Y., Tectonic features and evolution of the western Kunlun Mountain region, (in Chinese with English abstract), *Sci. Geol. Sinica*, *3*, 224–232, 1990.

Pan, Y., Unroofing history and structural evolution of the southern Lhasa terrane, Tibetan Plateau: Implications for the continental collision between India and Asia, Ph.D. thesis, 287 pp., State Univ. of N. Y., Albany, 1993.

Pearce, J. A., and W. Deng, The ophiolites of the Tibetan Geotraverses, Lhasa to Golmud (1985) and Lhasa to Kathmandu (1986), *Philos. Trans. R. Soc. London, Ser. A*, *327*, 215–238, 1988.

Pearce, J. A., and H. Mei, Volcanic rocks of the 1985 Tibet Geotraverse: Lhasa to Golmud, *Philos. Trans. R. Soc. London, Ser. A*, *327*, 169–201, 1988.

Peltzer, G., and P. Tapponnier, Formation and evolution of strike-slip faults, rifts, and basins during the India-Asia collision: An experimental approach, *J. Geophys. Res.*, *93*, 15,085–15,117, 1988.

Powell, C. M., and P. J. Conaghan, Plate tectonics and the Himalayas, *Earth Planet. Sci. Lett.*, *20*, 1–12, 1973.

Quidelleur, X., M. Grove, O. M. Lovera, T. M. Harrison, and A. Yin, Thermal evolution and slip history of the Renbu-Zedong Thrust, southeastern Tibet, *J. Geophys. Res.*, *102*, 2659–2679, 1997.

Ratschbacher, L., W. Frisch, G. Liu, and C. C. Chen, Distributed deformation in southern and western Tibet during and after the India-Asian collision, *J. Geophys. Res.*, *99*, 19,917–19,945, 1994.

Renne, P. R., A. L. Deino, R. C. Walter, B. D. Turrin, C. C. Swisher, T. A. Becker, G. H. Curtis, W. D. Sharp, and A. R. Jaouni, Intercalibration of astronomical and radioisotopic time, *Geology*, *22*, 783–786, 1994.

Royden, L. H., B. C. Burchfiel, R. W. King, E. Wang, C. Zhiliang, S. Feng, and L. Yuping, Surface deformation and lower crustal flow in eastern Tibet, *Science*, *276*, 788–790, 1997.

Schelling, D., The tectonostratigraphy and structure of the eastern Nepal Himalaya, *Tectonics*, *11*, 925–943, 1992.

Schuhmacher, M., E. de Chambost, K. D. McKeegan, T. M. Harrison, and H. N. Migeon, In situ U/Pb dating of zircon with the CAMECA IMS 1270, in *Secondary Ion Mass Spectrometry SIMS IX*, edited by A. Benninghoven et al., pp. 912–922, Wiley, New York, 1994.

Searle, M. P., Cooling history, erosion, exhumation, and kinematics of the Himalaya-Karakoram-Tibet orogenic belt, in *The Tectonic Evolution of Asia*, edited by A. Yin and T. M. Harrison, pp. 110–137, Cambridge Univ. Press, New York, 1996a.

Searle, M. P., Geological evidence against large-scale pre-Holocene offsets along the Karakoram Fault:

Implications for the limited extrusion of the Tibetan plateau, *Tectonics*, *15*, 171–186, 1996b.

Searle, M. P., R. F. Weinberg, and W. J. Dunlap, Transpressional tectonics along the Karakoram fault zone, northern Ladakh: constraints on Tibetan extrusion, in *Continental Transpressional and Transtensional Tectonics*, vol. 135, edited by R. E. Holdsworth, R. A. Strachan, and J. F. Dewey, *Geol. Soc. Spec. Publ., 135*, 307–326, 1998.

Searle, M. P., M. A. Khan, J. E. Fraser, S. J. Gough, and M. Q. Jan, The tectonic evolution of the Kohistan-Karakoram collision belt along the Karakoram Highway transect, north Pakistan, *Tectonics*, *18*, 929–949, 1999.

Shen, F., L. H. Royden, and B. C. Burchfiel, Large-scale crustal deformation of the Tibetan Plateau, *J. Geophys. Res.*, *106*, 6793–6816, 2001.

Srimal, N., India-Asia collision: Implications from the geology of the eastern Karakoram, *Geology*, *14*, 523–527, 1986.

Srivastava, P., and G. Mitra, Thrust geometries and deep structure of the outer and lesser Himalaya, Kumaon and Garhwal (India): Implications for evolution of the Himalayan fold-and-thrust belt, *Tectonics*, *13*, 89–109, 1994.

Stacey, J. S., and J. D. Kramers, Approximation of terrestrial lead isotope evolution by a two-stage model, *Earth Planet. Sci. Lett.*, *26*, 207–221, 1975.

Tang, Y., and F. Wang, Primary analysis of the tectonic environment of the ophiolite in Northern Xizang, *Himalayan Geol.*, *2*, 99–113, 1984.

Tapponnier, P., et al., The Tibetan side of the India-Eurasia collision, *Nature*, *294*, 405–410, 1981.

Tapponnier, P., G. Peltzer, A. Y. Le Dain, R. Armijo, and P. Cobbold, Propagating extrusion tectonics in Asia: New insights from simple experiments with plasticine, *Geology*, *10*, 611–616, 1982.

Tapponnier, P., Z. Xu, F. Roger, B. Meyer, N. Arnaud, G. Wittlinger, and J. Yang, Oblique stepwise rise and growth of the Tibet Plateau, *Science*, *294*, 1671–1677, 2001.

Taylor, M., A. Yin, F. J. Ryerson, P. Kapp, and L. Ding, Conjugate strike-slip faulting along the Bangong-Nujiang suture zone accommodates coeval east-west extension and north-south shortening in the interior of the Tibetan Plateau, *Tectonics*, *22*, doi:10.1029/2001TC001362, in press, 2003.

Van der Woerd, J., F. J. Ryerson, P. Tapponnier, Y. Gaudemer, R. Finkel, A. S. Meriaux, M. Caffee, Z. Guoguang, and H. Qunlu, Holocene left-slip rate determined by cosmogenic surface dating on the Xidatan segment of the Kunlun fault (Qinghai, China), *Geology*, *26*, 695–698, 1998.

Wang, S., Z. Li, and X. Qiangba, Geologic map and geologic report of the Xigaze area, Tibetan Bur. of Geol. and Miner. Resour., Llasa, 1983.

Xu, R. H., U. Schärer, and C. J. Allègre, Magmatism and metamorphism in the Lhasa block (Tibet): A geochronological study, *J. Geol.*, *93*, 41–57, 1985.

Yin, A., Mode of Cenozoic east-west extension in Tibet suggesting a common origin of rifts in Asia during the Indo-Asian collision, *J. Geophys. Res.*, *105*, 21,745–21,759, 2000.

Yin, A., and T. M. Harrison, Geologic Evolution of the Himalayan-Tibetan Orogen, *Annu. Rev. Earth Planet. Sci.*, *28*, 211–280, 2000.

Yin, A., T. M. Harrison, F. J. Ryerson, W. J. Chen, W. S. F. Kidd, and P. Copeland, Tertiary structural evolution of the Gangdese thrust system in southeastern Tibet, *J. Geophys. Res.*, *99*, 18,175–18,201, 1994.

Yin, A., T. M. Harrison, M. A. Murphy, M. Grove, S. Nie, F. J. Ryerson, X. F. Wang, and Z. L. Chen, Tertiary deformation history of southeastern and southwestern Tibet during the Indo-Asian collision, *Geol. Soc. Am. Bull.*, *111*, 1644–1664, 1999a.

Yin, A., P. A. Kapp, M. A. Murphy, T. M. Harrison, M. Grove, L. Ding, X. Deng, and C. Wu, Significant late Neogene east-west extension in northern Tibet, *Geology*, *27*, 787–790, 1999b.

Yin, J., J. Xu, C. Liu, and H. Li, The Tibetan plateau: Regional stratigraphic context and previous work, *Philos. Trans. R. Soc. London, Ser. A*, *327*, 5–52, 1988.

Zhang, K. J., Cretaceous palaeogeography of Tibet and adjacent areas (China): Tectonic implications, *Cretaceous Res.*, *21*, 23–33, 2000.

Zhao, W.-L., and W. J. Morgan, Injection of Indian crust into Tibetan lower crust: A two-dimensional finite element model study, *Tectonics*, *6*, 489–504, 1987.

Zhou, M.-F., J. Malpas, P. T. Robinson, and P. H. Reynolds, The dynamothermal aureole of the Donqiao ophiolite (northern Tibet), *Can. J. Earth Sci.*, *34*, 59–65, 1997.

---

L. Ding and J. Guo, Institute of Geology and Geophysics, Lithosphere Tectonic Evolution Laboratory, Chinese Academy of Sciences, Beijing 100029, People's Republic of China. (dinglin@mail.igcas.ac.cn)

P. Kapp, Department of Geosciences, University of Arizona, Gould-Simpson Building, Tucson, AZ 85721-0077, USA. (pkapp@geo.arizona.edu)

T. M. Harrison and A. Yin, Department of Earth and Space Sciences and Institute of Geophysics and Planetary Physics, University of California, Los Angeles, CA 90095-1567, USA. (tmh@argon.ess.ucla.edu; yin@ess.ucla.edu)

M. A. Murphy, Department of Geosciences, University of Houston, Houston, TX 77204-5007, USA. (mmurphy@mail.uh.edu)


**Figure 4.** (a) View to north at flat-lying, columnar-jointed volcanic rocks overlying tilted red beds. The sample dated in this study (PK7-16-2) was collected from this exposure. (b) View of Narangjiapo and Zaduo thrusts looking toward southeast from near sample locality 7-14-1 (Foldout 1). The Narangjiapo thrust juxtaposes steeply dipping beds of Permian strata in the hanging wall against Cretaceous volcanic and volcaniclastic rocks in the footwall. Here, the Zaduo thrust is north dipping and places ophiolitic melange over Cretaceous rocks to the south. (c) Photo of Zaduo thrust taken from granite outcrop near locality 7-5-3 and looking toward the east-southeast. Here, it juxtaposes ophiolitic melange (dark-colored) in its hanging wall against Permian limestone and sandstone (gray) in its footwall. The fault zone is characterized by a resistant rib of orange fault breccia. (d) A view from ~2 km northeast of Shiquanhe (Foldout 1) toward the east-southeast along the trace of the Shiquanhe thrust. Here, the thrust juxtaposes Permian strata and the Longzi La granite in the hanging wall against green (Tc2) and red (Tc1) nonmarine basin fill in its footwall.